Turkish Journal of Earth Sciences

Volume 32 | Number 6 Article 5

9-29-2023

Mineralogical-petrographical features, geochemical characteristics, and S isotope variability of Pb-Zn deposits in the Sakarya fragment of the Biga Peninsula (NW Türkiye)

GÖKHAN DEMİRELA

SİNAN AKISKA

ELİF AKISKA

Follow this and additional works at: https://journals.tubitak.gov.tr/earth

 Part of the Earth Sciences Commons

Recommended Citation

DEMİRELA, GÖKHAN; AKISKA, SİNAN; and AKISKA, ELİF (2023) "Mineralogical-petrographical features, geochemical characteristics, and S isotope variability of Pb-Zn deposits in the Sakarya fragment of the Biga Peninsula (NW Türkiye)," *Turkish Journal of Earth Sciences*: Vol. 32: No. 6, Article 5. https://doi.org/10.55730/1300-0985.1874

Available at: https://journals.tubitak.gov.tr/earth/vol32/iss6/5

This Article is brought to you for free and open access by TÜBİTAK Academic Journals. It has been accepted for inclusion in Turkish Journal of Earth Sciences by an authorized editor of TÜBİTAK Academic Journals. For more information, please contact academic.publications@tubitak.gov.tr.

Turkish Journal of Earth Sciences

http://journals.tubitak.gov.tr/earth/

Research Article

Turkish J Earth Sci
(2023) 32: 772-807
© TÜBİTAK
doi:10.55730/1300-0985.1874

Mineralogical-petrographical features, geochemical characteristics, and S isotope variability of Pb-Zn deposits in the Sakarya fragment of the Biga Peninsula (NW Türkiye)

Gökhan DEMİRELA[1], Sinan AKISKA[2,*], Elif AKISKA[2]

[1]Department of Geological Engineering, Aksaray University, Aksaray, Turkiye
[2]Department of Geological Engineering, Ankara University, Ankara, Turkiye

Received: 06.09.2022 • **Accepted/Published Online:** 17.07.2023 • **Final Version:** 29.09.2023

Abstract: The Biga Peninsula in northwestern Anatolia, a part of the Alpine-Himalayan orogenic belt, has a complex geology that was formed following the closure of the northern branch of the Neotethys. Intense volcanism and plutonism in the area from the Eocene to the Middle Miocene period caused several Pb-Zn-Cu±Ag±Au deposits to form. The geometry of the mineralizations is largely made up of polymetallic veins, manto-chimneys, and irregular replacement bodies. Ore-bearing and host rocks in the mineralization zones and the wall rocks outside the mineralization zones were compiled in this study. The most common minerals in the skarn zones are garnet, pyroxene, amphibole, epidote, chlorite, quartz, and calcite, while quartz, calcite, and sericite are formed in the hydrothermal alteration zones. Based on the geochemical analyses, the granitoidic rocks are granodiorite, whereas the volcanic rocks are dacite, andesite, trachyandesite, and basaltic andesite. According to the skarn-forming features, the Biga plutons have chemical characteristics that can form Pb-Zn, Cu, Fe, and Au skarns.

The carbonate units in the area are made up of marble (fresh), marble (in the alteration zone), and ore calcite. The geochemical analyses of the carbonate units indicate that in composition the fresh marble is almost pure $CaCO_3$. However, the marble in the alteration zone has higher SiO_2, Fe_2O_3, MgO, and MnO contents than that of the fresh marble. These values are higher in ore calcite. The metasandstones mostly consist of arkose and may have contributed to the main mineralization as they have initial ore element enrichment. According to a hierarchical cluster analysis (HCA) result, three different element groups were detected, these being Sb, Rb, Zr, Ag, Y, Mo, Hg, and Nb (increased during alteration), Sr and Ba (decreasing in alteration), and Cu, Au, As, and Cd (mineralization-related). Rare earth element (REE) characteristics indicate that hydrothermal fluids, responsible for the formation of the Biga Peninsula Pb-Zn deposits, are characterized by very low REE concentrations, and consequently the origin of these fluids is predominantly meteoric. The ∑REE, $(Pr/Yb)_{cn}$, Ce/Ce* values (8.63–24.79 ppm, 2.84–8.23, 0.38–0.82, respectively) of the marble in the alteration zone and ore-bearing skarns (3.34–27.20 ppm, 2.32–5.87, 0.36–0.83) support the findings of the meteoric contribution. Based on the similarities of the general trends and the abundances of REE elements in ore-bearing skarns and wall rocks, it is thought that wall rocks may have contributed part of the lead. The $\delta^{34}S$ isotope compositions of galena, sphalerite, pyrite, and chalcopyrite fall into a narrow range of around 0‰. This data indicates that the sulfur in the Pb-Zn±Cu sulfides in the Biga Peninsula is of magmatic origin ($\delta^{34}S_{min}$: –5.5, $\delta^{34}S_{max}$: 5.2, $\delta^{34}S_{avg}$: –0.7; n: 40). According to the $\delta^{34}S$ values, the mineralizations occurred under intermediate sulfidation conditions, in a reducing environment with H_2S-dominant fluids with a near neutral pH value.

Key words: Tethyan Metallogenic Belt, hydrothermal, skarn, rare earth elements, S isotope

1. Introduction

The primary aim in the genetical investigation of skarn and hydrothermal deposits is to determine the source of ore fluids and the various isotope methods (e.g., H, Li, B, C, N, O, S) are used for this purpose (e.g., Rye and Ohmoto, 1974; Taylor, 1997; Huston, 1999; Tomascak, 2004; Seal, 2006). However, these methods are not enough when detecting the origin of the ore. Detailed mineralogy and petrography findings, mineral chemistry, and fluid inclusion studies should also be provided for determining the genesis of ore and related fluid(s). Trace and rare earth element (REE) compositions of hydrothermal fluids and host rocks provide useful information concerning the origin of ore-forming elements, including base metals (Kato, 1999). Due to their similar physical and chemical characteristics, REEs behave in a similar manner in many geological processes (Taylor and McLennan, 1985). REE patterns normalized with standard materials play an important

* Correspondence: akiska@eng.ankara.edu.tr

This work is licensed under a Creative Commons Attribution 4.0 International License.

role in the detection of various geochemical processes. The number of studies conducted in order to determine the origin of ore-forming hydrothermal fluids using trace element and REE contents have increased in recent years. Kato (1999) specified that REEs can be used as indicators to detect the origin of skarn deposits and found a close relationship between hydrothermal fluids and ∑REE, $(Pr/Yb)_{cn}$, Ce/Ce*, Eu/Eu* values in several deposits in Japan. Qicong and Congqiang (2003) examined the behavior of both trace elements and REEs in skarns and found that high field strength elements (HFSE) such as Zr, Hf, Th, and Nb were immobile in the formation of skarns, while other trace elements were mobile. Tao et al. (2012) noted that the REE patterns of ore calcites in the Langdu Cu-skarn deposit (Zhongdian Area, Yunnan Province) are unique, with a heavy rare earth elements (HREE)-rich, light rare earth elements (LREE)-depleted, and relatively high Eu anomaly. Zamanian and Radmard (2016) investigated the REE characteristics of ore zone and plutons related to the Baba Ali (Iran) skarn deposit. The authors, using the $(Pr/Yb)_{cn}$, Ce/Ce* and Eu/Eu* parameters stated by Kato (1999), found that the fluids forming the epidote and garnet are primarily of magmatic origin, whereas the magnetite, actinolite, and phlogopite are of magmatic origin (with low-REE concentration) or meteoric origin. Orhan and Mutlu (2017) determined the features of the exoskarn zone by using the major oxide and trace element characteristics of skarn facies in the Kozbudaklar W-skarn deposit (Bursa, Türkiye). In addition, the REE characteristics of the skarn zone were compared with those of the host rocks (pluton and marble). Also, the physicochemical conditions during mineralization were discussed (Orhan and Mutlu, 2017).

Metamorphic basement rocks and Cenozoic volcanics and subvolcanics are the host rocks of the Pb-Zn±Cu±Ag mineralizations in the Sakarya fragment of the Biga Peninsula (e.g., Demirela, 2011; Yiğit, 2012; Akıska et al., 2013; Demirela et al., 2014; Bozkaya and Banks, 2015; Akıska, 2020; Demirela and Akıska, 2022). These mineralizations are typically found in the carbonate levels of metamorphic rocks, fractures in volcanics-subvolcanics and metamorphic rocks, and rarely along volcanic-metamorphic rock contacts (e.g., Bozkaya, 2011; Demirela, 2011; Yigit, 2012; Akıska, 2020). Recent studies in the region have focused on two ore zones at the Arapuçandere mineralization and Handeresi Ore District (Kalkım mineralizations).

Geology, mineralogy, and fluid inclusion, radiogenic isotope (Pb) and stable isotope data (S, H-O isotopes) of Arapuçandere Pb-Zn-Cu-Ag deposit have been reported in a number of studies (Örgün et al., 2005; Bozkaya et al., 2008; Bozkaya, 2011; Bozkaya and Banks, 2015; Çiçek et al., 2021). According to these studies, the deposit consists of epithermal base metal mineralization, while the origin of the fluids is predominantly meteoric, along with some magmatic-meteoric fluid traces. The sulfur mainly derived from a magmatic source, while a considerable amount of lead was also sourced from the wall rocks (Bozkaya, 2011; Bozkaya and Banks, 2015). However, Çiçek et al. (2021) argued that the source of the sulfur and metals of Arapuçandere and the surrounding Pb-Zn mineralizations were Oligo-Miocene granitoids with no contribution from the wall rocks.

Several studies have investigated the Handeresi, Bağırkaçdere, Çulfa Çukuru, and Karaaydın Pb-Zn-Cu±(Ag-Au) mineralizations in the Handeresi Ore District (Akıska et al., 2013; Akıska and Demirela, 2014; Akıska, 2020). Geological-mineralogical, fluid inclusion, mineral chemistry, radiogenic (Pb), and stable isotope (S, C-O) investigations were carried out in these studies. The authors noted that the mineralizations have similar characteristics with distal type Pb-Zn skarn systems. The source of the sulfur is magmatic, while lead was derived from a magmatic source, mixed with a minor amount of lead from the wall rocks (schist and metasandstone).

These mineralizations have been examined based on the mineralogical, petrographical features, fluid inclusion, mineral chemistry, and isotope systematics of the ore-alteration zones (e.g., Bozkaya et al., 2008; Bozkaya and Gökçe, 2009; Bozkaya, 2011; Akıska et al., 2013; Akıska and Demirela, 2014; Çiçek et al., 2021). However, the geochemical characteristics of the ore-bearing alteration zone and wall rocks as well as S isotope characteristics of sulfide minerals have yet to be comparatively investigated. This study presents the geochemical features of the schist, metasandstone, marble, volcanic, and plutonic rocks related to the Pb-Zn mineralizations of the Sakarya fragment in the Biga Peninsula. Several studies have previously been carried out on the geotectonic features and geodynamic evolution of the Biga igneous rocks (e.g., Delaloye and Bingöl, 2000; Altunkaynak and Genç, 2008; Altunkaynak et al., 2012). However, this study is the first to describe and interpret the mineralization characteristics of the igneous rocks as well as the geochemical features of fresh marble, ore zone marble, ore calcite, and wall rocks. This study also aimed to shed light on the physicochemical conditions of mineralization using S isotope data.

2. Regional geology and Pb-Zn mineralizations

The Biga Peninsula, an important part of the Tethyan Metallogenic Belt, is located in the Alpine Orogenic System of northwestern Türkiye. According to Ketin (1966), the Biga Peninsula is tectonically located within the Pontide tectonic belt and forms the western end of this belt. The boundaries of this belt, referred to as the Sakarya Continent by Şengör and Yılmaz (1981), are known as the Intra-Pontide Suture in the north and the İzmir-Ankara

Suture in the south. Okay (1984, 1989) extended the eastern border of the Sakarya Zone to the east to include the Eastern Pontides, as it possessed similar stratigraphic and tectonic development to that of northwest Anatolia.

The Biga Peninsula was formed by high-medium degree metamorphic, ophiolite, plutonic, volcanic, and sedimentary rocks. Carboniferous Kazdağ Massif rocks, which were metamorphosed under amphibolite and granulite facies conditions (Okay and Satır, 2000a, 2000b; Duru et al., 2004; Yaltırak and Okay, 2004; Cavazza et al., 2009), Çamlıca and Karabiga metamorphic units (Beccaletto et al., 2007; Şengün and Çalık, 2007; Şengün et al., 2011, Aygül et al., 2012), the Permo-Triassic Karakaya Complex (Okay et al., 1990), and the Cretaceous ophiolitic mélanges (the subduction-accretion Çetmi mélange: Middle Cretaceous - Okay et al., 1990; Beccaletto et al., 2005 and Denizgören ophiolite: Lower-Middle Cretaceous - Okay et al., 1990; Beccaletto and Jenny, 2004) form the basement of the peninsula (Siyako et al., 1989; Okay et al., 1990; Dönmez et al., 2005, 2008; Altunkaynak and Genç, 2008; Dilek et al., 2009; Altunkaynak et al., 2012) (Figure 1). The region was shaped by intense magmatism beginning from the Eocene until the Quaternary in three pulses. The first episode during the Eocene produced both volcanic and plutonic rocks in the north and northwestern part of the peninsula (Harris et al., 1994; Genç and Yılmaz, 1997; Köprübaşı and Aldanmaz, 2004; Altunkaynak, 2007; Karacık et al., 2008). The second episode during the Oligo-Miocene resulted in the formation of volcanics and coeval granitoid plutons, similar to those of the Eocene igneous units (Seyitoğlu and Scott, 1992, 1996; Genç and Yılmaz 1997; Aldanmaz et al., 2000; Yılmaz et al., 2000; Altunkaynak and Dilek, 2006; Erkül, 2010; Altunkaynak et al., 2012; Aysal, 2015; Aysal et al., 2021). The third episode during the Late Miocene-Quaternary produced mainly alkaline volcanic units of intraplate origin (Siyako et al., 1989; Yılmaz, 1989, 1990; Güleç, 1991; Yılmaz and Polat, 1998; Aldanmaz et al., 2006). During the first two episodes, granitoidic rocks intruded into the basement rocks whereas andesite, trachyandesite, dacite, rhyodacite, and rhyolite cut the basement rocks and covered these units unconformably. In the Cenozoic period, intense sedimentation occurred in the Biga Peninsula, often contemporaneous with volcanic activity. All units were unconformably covered by Plio-Quaternary lacustrine and fluvial deposits (Duru et al., 2004) (Figure 1).

Metamorphic and volcanic rocks outcropping in the close vicinity of the granitoid intrusions in the Biga Peninsula are the host rocks of Pb-Zn±Cu±Ag mineralizations like many similar ore mineralizations in the region (e.g., Wagner et al., 1985; Örgün et al., 2005; Demirela, 2011; Akıska, 2020; Çiçek et al., 2021; Demirela

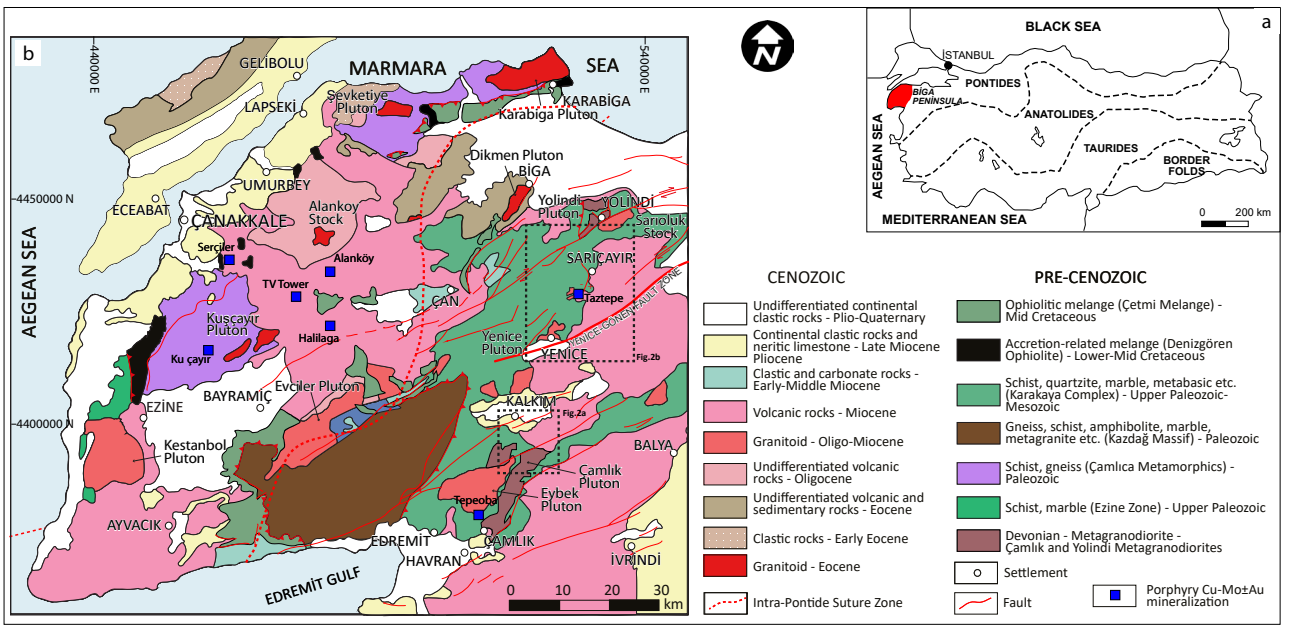


Figure 1. Generalized geological map of the Biga Peninsula (Siyako et al., 1989; Okay et al., 1990; Duru et al., 2012) (please see the details of porphyry deposits in Kuşcu et al., 2019 and references therein).

and Akıska, 2022). The mineralization characteristics and formation conditions of these deposits were given in Akıska (2020) and Demirela and Akıska (2022) in detail. To avoid repetition, a brief summary of the deposits was given below.

These mineralizations were aligned parallel to the Yenice-Gönen fault as structurally controlled or formed in the carbonate units (marble, calc-schist) as lithologically controlled. Çağatay (1980) and Anıl (1984) conducted genetic classifications of Pb-Zn deposits in the Biga Peninsula. In recent studies, the Pb-Zn±Cu±Ag mineralizations were divided into two separate groups and reexamined, taking into account the lithological properties of the host rocks and the structural features of the mineralizations (Demirela 2011; Akıska, 2020; Demirela and Akıska, 2022).

The first type of mineralization, formed through metasandstone, quartzite, metadiabase, and schist including marble lenses, can be seen in the close vicinity of the Cenozoic granitoids in the Sakarya fragment of the Biga Peninsula. These are skarn-replacement type Pb-Zn±Cu±Ag deposits including the Handeresi, Sameteli, Umurlar, Sarıçayır, and Alandere mineralizations (Figures 2a and 2b). The second type of mineralization developed either along with the fractures of diabase, metasandstone, and schist belonging to the basement of the Biga Peninsula or in the Cenozoic volcanics in the region. Kurttaşı, Sofular, Gümüşler, and Arapuçandere mineralizations, which are particularly common around the Yenice district, are the most notable examples of these types of deposits (Figures 2a and 2b).

3. Analytical methods

Within the scope of the field studies, a total of 225 rock samples were taken from the field and thin sections were prepared from 185 samples in the Thin Section and Polishing Laboratory of the Department of Geological Engineering in Ankara University. Thin sections were examined under a Leica DM/LSP polarizing microscope and petrographic definitions were made. Photographs were taken to reflect the mineralogical composition and textural features of key sections. Geochemical analysis was carried out on 8 samples of ore-bearing skarns and 45 samples of wall rocks (Table 1). After the samples were cut into pieces with a hammer, they were crushed below 0.5 cm with a jaw crusher. All broken samples were ground under 200 mesh in a Fritsch brand grinder. Samples weighing around 20 grams were placed in nylon bags sent

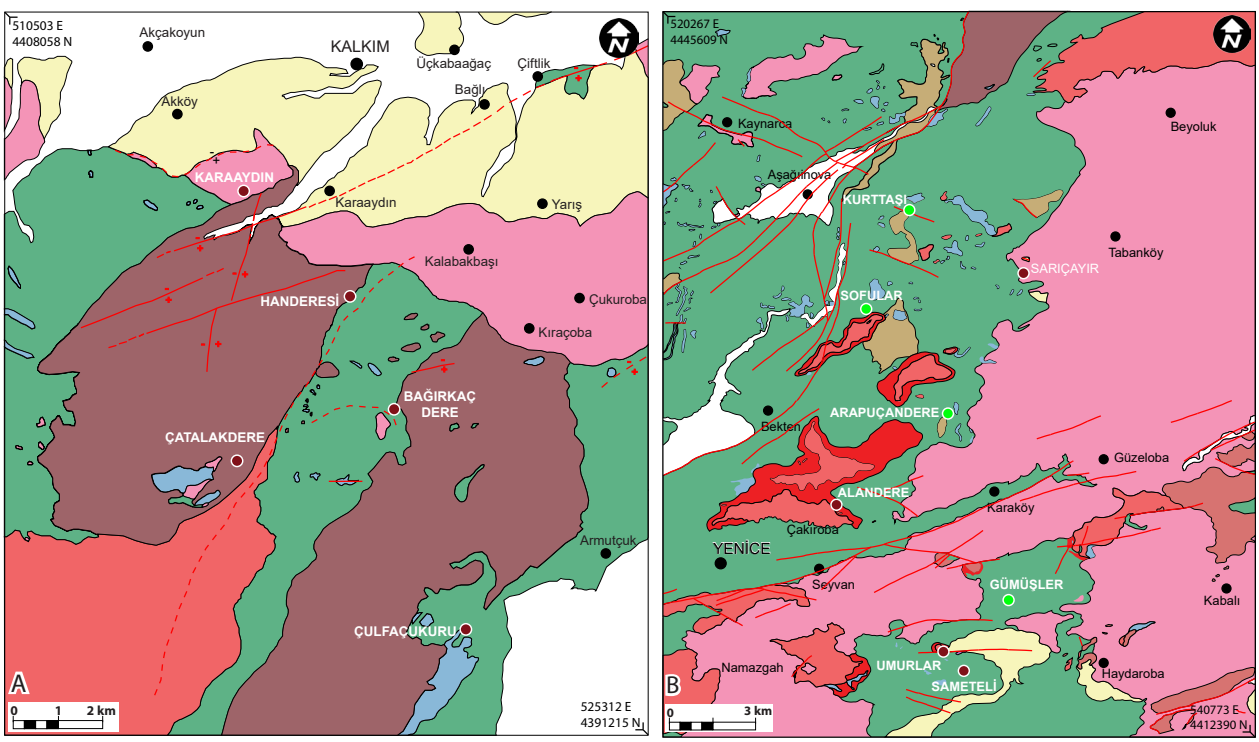


Figure 2. A. Southern part of the Yenice Pb-Zn mineralizations (Handeresi Ore District), B. the western and northern part of the Yenice Pb-Zn mineralizations (Siyako et al., 1989; Okay et al., 1990; Duru et al., 2012). (The coordinates are given in UTM coordinate system, Zone: 35N.) (Dark red points indicate Pb-Zn skarn mineralizations while green points indicate hydrothermal Pb-Zn mineralizations.)

Table 1. Sampling points of ore-bearing skarns and wall rocks of the Sakarya Pb-Zn fragment in the Biga Peninsula. (All coordinate values were given as UTM Zone 35N.)

	Sample#	Unit	Location	Easting	Northing
1	CC07_2_27	Marble (fresh)	Handeresi Ore District	521112	4394358
2	DD13-04	Marble (fresh)	Handeresi Ore District	514383	4401901
3	SAM13-04A	Marble (fresh)	Sameteli	531050	4415418
4	SARY13-02	Marble (fresh)	Sarnıçköy-Yolindi	528991	4442786
5	AD13-07	Marble (in the ore zone)	Alandere	526916	4423541
6	AU13-09	Marble (in the ore zone)	Arapuçandere	530306	4426905
7	DD13-02A	Marble (in the ore zone)	Handeresi Ore District	511430	4401671
8	SAM13-06A	Marble (in the ore zone)	Sameteli	530876	4415498
9	KA13-01	Ore calcite	Kurttaşı-Aşağıinova	525840	4435653
10	CC07_2_26	Ore calcite	Handeresi Ore District	521080	4394290
11	CO13-02	Granodiorite	Çakıroba	525036	4422599
12	CO13-03	Granodiorite	Çakıroba	524554	4422870
13	CO13-04	Granodiorite	Çakıroba	523643	4422703
14	YO13-01	Granodiorite	Yolindi	533795	4441968
15	YO13-02	Granodiorite	Yolindi	535015	4442227
16	CC07_2_10	Granodiorite	Handeresi Ore District	520055	4393350
17	AU13-10	Trachy andesite-andesite	Arapuçandere	531948	4426822
18	CC07_2_28	Granodiorite porphyry	Handeresi Ore District	521072	4393854
19	KAL-12	Andesite porphyry	Kalkım	524078	4400398
20	KAL-13	Andesite porphyry	Kalkım	524106	4398804
21	KAL-16	Andesite	Kalkım	525575	4402741
22	KS13-01	Andesite	Karaköy-Soğucak	533045	4425976
23	KS13-02	Andesite	Karaköy-Soğucak	532480	4424156
24	KS13-03	Andesite	Karaköy-Soğucak	532414	4427365
25	CAT10-04B	Andesite	Handeresi Ore District	517418	4400005
26	CC07_2_29	Andesite	Handeresi Ore District	519989	4392098
27	CC07_2_32	Andesite	Handeresi Ore District	520939	4393187
28	CC07_12	Andesite	Handeresi Ore District	520980	4394200
29	ASA13-02	Garnet-sericite graphite schist	Aşağıinova-Sarnıçköy	526484	4440055
30	CC07_2_17	Graphite-sericite schist	Handeresi Ore District	521837	4395387
31	GUM13-03	Sericite-graphite schist	Gümüşler	531421	4417307
32	MEN14	Sericite-graphite schist	Handeresi Ore District	519617	4398715
33	SAM13-02	Sericite-graphite schist	Sameteli	530778	4415422
34	SK13-01	Sericite-graphite schist	Sarıçayır-Kurttaşı	531345	4434205
35	YY13-01	Sericite-graphite schist	Yenice	530030	4420554
36	ALD13-01	Sericite-graphite schist	Alandere	526776	4423935
37	CO13-05	Sericite schist	Çakıroba	522393	4424293
38	SS13-01	Sericite schist	Soğucak-Sarıçayır	528150	4431712
39	CC07_2_9	Ore-bearing graphite schist	Handeresi Ore District	520220	4393362
40	CAT10-02	Metasandstone	Handeresi Ore District	517357	4399888
41	CAT10-09A	Metasandstone	Handeresi Ore District	517393	4400018

Table 1. (Continued)

	Sample#	Unit	Location	Easting	Northing
42	CC07_2_18	Metasandstone	Handeresi Ore District	520825	4394380
43	CC07_2_30	Metasandstone	Handeresi Ore District	520016	4392194
44	AD13-08	Metasandstone	Alandere	526916	4423541
45	SO13-01	Metasandstone	Sofular-Kurttaşı	528045	4433301
46	CC07_2_23	Ore bearing skarn	Handeresi Ore District	521038	4394233
47	SAM13-03	Ore bearing skarn	Sameteli	530876	4415498
48	CC07_2_36	Ore bearing skarn	Handeresi Ore District	521072	4393854
49	GUM13-07	Ore bearing skarn	Gümüşler	532039	4418025
50	AD13-03	Ore bearing skarn	Alandere	526868	4423751
51	AD13-04	Ore bearing skarn	Alandere	526872	4423697
52	CD13-01	Ore bearing skarn	Handeresi Ore District	517002	4399995
53	CC07_2_7	Ore bearing skarn	Handeresi Ore District	520707	4393810

to Canadian Bureau Veritas Analysis Laboratories (ACME Lab) for major, trace, and rare earth element analysis. In the laboratory the samples were analyzed using the ICP-ES method for major element compositions and the ICP-MS method for trace element compositions. The prepared sample was mixed with $LiBO_2/Li_2B_4O_7$ flux. Crucibles are fused in a furnace. The cooled bead was dissolved in ACS grade nitric acid and analyzed by ICP and/or ICP-MS. The loss on ignition (LOI) was determined by igniting a sample split and then measuring the weight loss.

A sulfur isotope study was carried out on a total of 40 samples selected from 7 Pb-Zn±Cu±Ag mineralizations (Handeresi Ore District, Sameteli Ore District, Alandere, Kurttaşı). This analysis was performed on galena, sphalerite, pyrite, and chalcopyrite samples at the Environmental Isotope Laboratory at the University of Arizona (USA). The samples selected for S isotope analyses were first ground and sieved to 2 mm. Individual grains were then separated using heavy liquids and handpicked under a binocular microscope. The $\delta^{34}S$ was measured on SO_2 gas in a continuous-flow gas-ratio mass spectrometer (ThermoQuest Finnigan Delta PlusXL). The samples were combusted at 1030 °C with O_2 and V_2O_5 using an elemental analyzer (Costech) coupled to the mass spectrometer. Standardization was based on international standards OGS-1 and NBS123, and several other sulfide and sulfate materials that were compared between laboratories. Calibration was linear in the range −10 to +30‰. Precision was estimated to be ±0.15 or better (1s), based on repeated internal standards.

4. Mineralogy-petrography

4.1. Metamorphic rocks

Schist, metasandstone, and marble belonging to the Karakaya Formation were outcropped in the study areas. Metasandstone and marble are seen as lenses in the schist.

Epidote-sericite-graphite schist and graphite schist have similar structural-textural features and are named differently due to their primary mineral differences. They are generally seen in dark green-black colors on a macroscopic scale (Figure 3a). Graphite and quartz-sericite which formed the schistosity are seen alternately in thin sections. The graphite grains are generally thready and aligned parallel to the schistosity (Figure 3b). Quartz is fine- to medium-grained and exhibits undulose extinction. In addition, secondary quartz was observed in the quartz and calcite veins that cut the metamorphic rocks. These are coarse-grained and euhedral-subhedral quartz crystals. Metamorphic epidote is fine-grained and often seen together with quartz (Figure 3b). Secondary epidotes (mostly clinozoisite or epidote in composition) were formed together with secondary quartz in the quartz and calcite veins. Sericite is very fine-grained and anhedral and is seen together with both graphite and quartz (Figure 3b).

The main mineralogical composition of chlorite schist is chlorite and quartz. This rock is generally fine-grained and has a distinctive schistosity. It is typically seen in green-dark gray colors on a macroscopic scale. Quartz and chlorite are fine- to medium-grained with trace amounts of sericite minerals in thin sections. Secondary quartz filled the fractures of the chlorite schist. A few pyrites were observed at the contact of these fractures and chlorite schist.

Calc-schist is mostly found in the adits of the Handeresi Ore District. This rock, having a distinctive schistosity, is generally seen with graphite schist and has a white – grayish-white color. Calcite is the major mineral with quartz as the minor. Both are very fine-grained

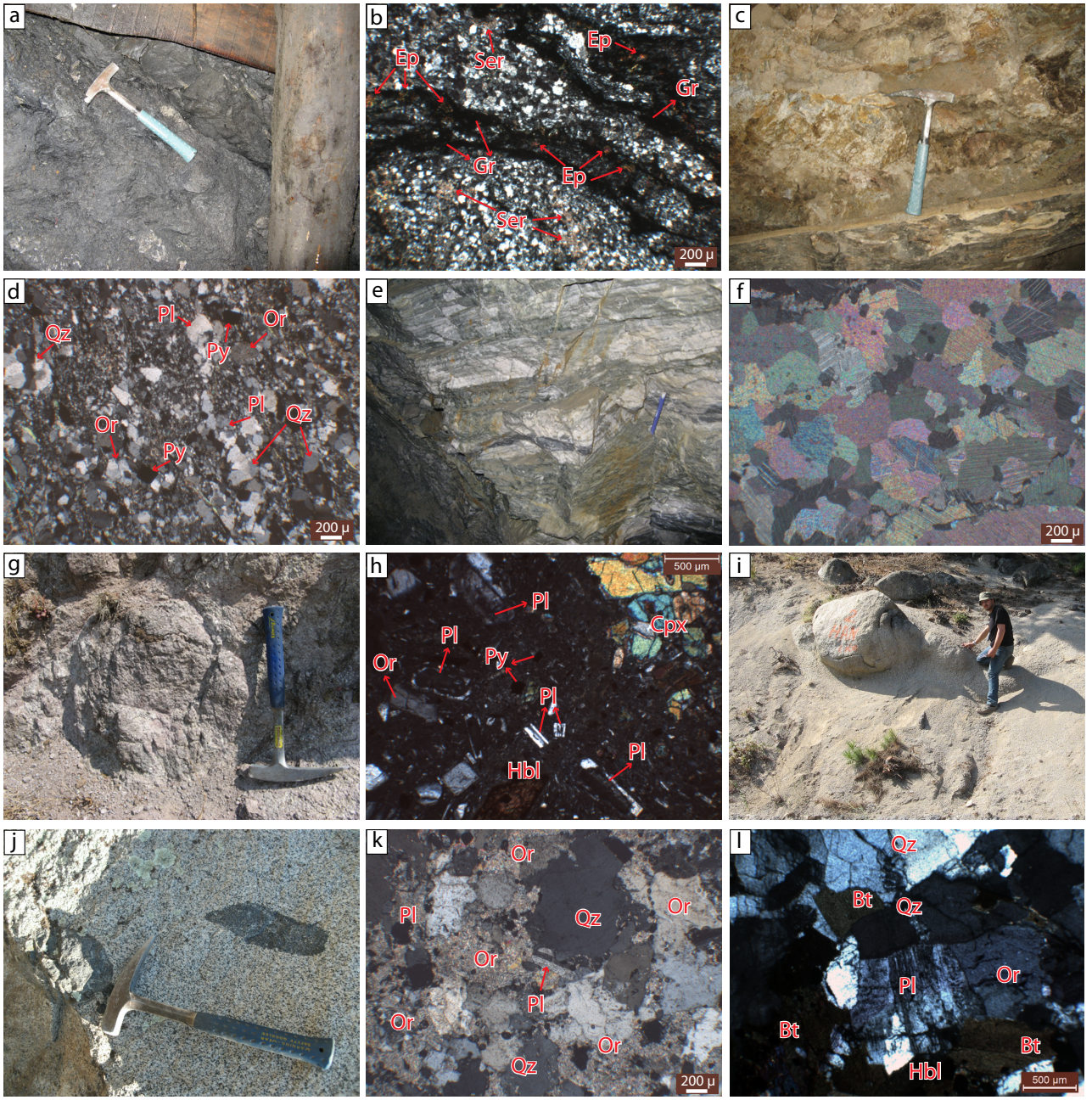


Figure 3. a. General view of the epidote-sericite-graphite schist in the ore adit (Çulfa Çukuru area), b. representative thin section image of the epidote-graphite-sericite schist (XPL), c. general view of the metasandstone (arkose) in the ore adit (Handeresi Ore District-Yarma adit), d. representative thin section image of the metasandstone (XPL), e. general view of the marble lenses in the ore adit (Handeresi Ore District-Bağırkaçdere Adit), f. representative thin section image of the marble (XPL), g. general view of the andesite in the field (Hallaçlar Formation), h. representative thin section image of the andesite (XPL), i. arenized granodiorites in the field (Eybek pluton), j. granodiorites including mafic enclaves (Çakıroba pluton), k. highly sericitized feldspar minerals (XPL), l. general view of the representative granodiorite thin section (XPL). (*Abbreviations: Bt: biotite, Cpx: clinopyroxene, Ep: epidote, Gr: graphite, Hbl: hornblende, Or: orthoclase, Pl: plagioclase, Py: pyrite, Qz: quartz, Ser: sericite.*)

and subhedral-anhedral. Occasionally, very fine-grained pyrites are aligned along the schistosity planes of these rocks.

Arkosic metasandstone with different thicknesses is observed as lenses in schists (Figure 3c). It is seen in yellow-brown colors on a macroscopic scale and has indistinct schistosity. The predominant minerals are quartz, plagioclase, and orthoclase found in thin sections (Figure 3d). The quartz is medium-grained and exhibits undulose extinction. The quantity of quartz is approximately the same as that of feldspar. Orthoclase is seen both as phenocrysts and in the matrix. Orthoclase in the matrix is fine-grained, whereas the orthoclase phenocryst is usually medium-grained and both show simple twinning. Plagioclase is present in small amounts and shows polysynthetic twins. Intensive sericitization was also identified in all feldspars. Medium-grained barren quartz veins/veinlets cut the metasandstone. A small number of pyrite and magnetite disseminations were also noticeable in thin sections.

White-gray-colored marble formed as lenses in schists in the study areas (Figure 3e) and is composed entirely of calcite. Medium-grained calcite is generally euhedral-subhedral and shows mosaic texture (Figure 3f). Quartz and epidote are present in small amounts. In the close vicinity of the mineralization zones, the calcite grains have coarser sizes due to recrystallization. Ore minerals were also observed in these zones.

4.2. Volcanic rocks

Porphyritic gray-pink volcanic rocks are andesite and trachyandesite (Figure 3g). Quartz, orthoclase, plagioclase, biotite, and amphibole are the main minerals. Altered andesites contain enclaves that include the same mineral composition. The matrix consists of volcanic glass and microliths and the mineralogical composition of the matrix could not be determined due to very fine-grained nature of the microliths and also due to intensive alteration. Quartz is medium- to coarse-grained and is the only mineral that did not show alteration in thin sections. Small amounts of quartz showing undulose extinction have embayed forms. Plagioclase is andesine to labradorite in composition, and is the most abundant feldspar. Plagioclase with variable grain sizes generally shows sericitization. The orthoclase, which shows simple twinning and perthitic texture, is usually medium-to coarse-grained. Hornblende and clinopyroxene were detected as mafic minerals (Figure 3h). Both the hornblende and clinopyroxene are euhedral-subhedral. There are also small quantities of opaque minerals in the andesites.

4.3. Plutonic rocks

Granodiorites are grayish at the mesoscopic and macroscopic scale and exhibit holocrystalline granular texture. They are mostly observed as arenized (Figure 3i) and they sometimes contain mafic enclaves (Figure 3j). The main minerals are quartz, orthoclase, plagioclase, biotite, hornblende, and rare pyroxene, whereas apatite, zircon, and titanite are the accessory minerals. Quartz exhibiting undulose extinction is medium- to coarse-grained and anhedral. The orthoclase, which shows simple twinning, is fine-medium grained and euhedral-subhedral. The plagioclase, oligoclase-andesine in composition, occurs as euhedral or subhedral phenocrysts and exhibits polysynthetic twinning. Some plagioclases have biotite and hornblende inclusions. Both the orthoclase and plagioclase are pervasively altered to clay and sericite (Figure 3k). Biotite forms tabular crystals has light-medium brown color and consists of basal cleavage (Figure 3l). Partly chloritization is developed in several biotites, and opaque minerals accompany the biotite seen together with the hornblende. Hornblende has green color and also shows a strong green-brown pleochroism and is characterized by perfect cleavage planes. Small amounts of pyroxene, mostly augite in composition, is colorless, euhedral-subhedral, and characterized by two perfect cleavages. Some pyroxenes partially altered to uralite.

4.4. Ore-bearing rocks

Mineralizations in the studied areas are observed both as hydrothermal veins (Figure 4a) in the metamorphic and volcanic rocks, and at the contact between marble and schist in the skarn zones (Figure 4b). Demirela and Akıska (2022) provided detailed explanations of the deposit types (epithermal high sulfidation (HS)/intermediate sulfidation (IS) Pb-Zn deposits and skarn/carbonate replacement (CR) Pb-Zn deposits). For this reason, only the mineralogical and petrographical investigations are provided here.

4.4.1. Epithermal Pb-Zn mineralizations

The main minerals are quartz, calcite, and sericite in the hydrothermal alteration zone. Quartz is the most abundant mineral in the hydrothermal veins and is euhedral coarse-grained. Quartz grains, seen with ore minerals, are up to several cm in size. Calcite accompanies the quartz, displays mosaic forms, and is euhedral-subhedral coarse-grained (Figure 4c). Sericite, mostly seen as euhedral-subhedral fine-grained, is observed with quartz in the hydrothermal veins. Sericite, accompanied by calcite and ore minerals, was formed only within ore-bearing veins. In addition, there are a few medium-coarse titanite crystals in veins.

Brecciation is observed in host rocks cut by hydrothermal veins (Figure 4d) and intense argillization and carbonatization are observed in felsic minerals. In some samples, the mineralizations were formed within the stockwork veins, which are surrounded by coarse-grained and euhedral-subhedral quartz.

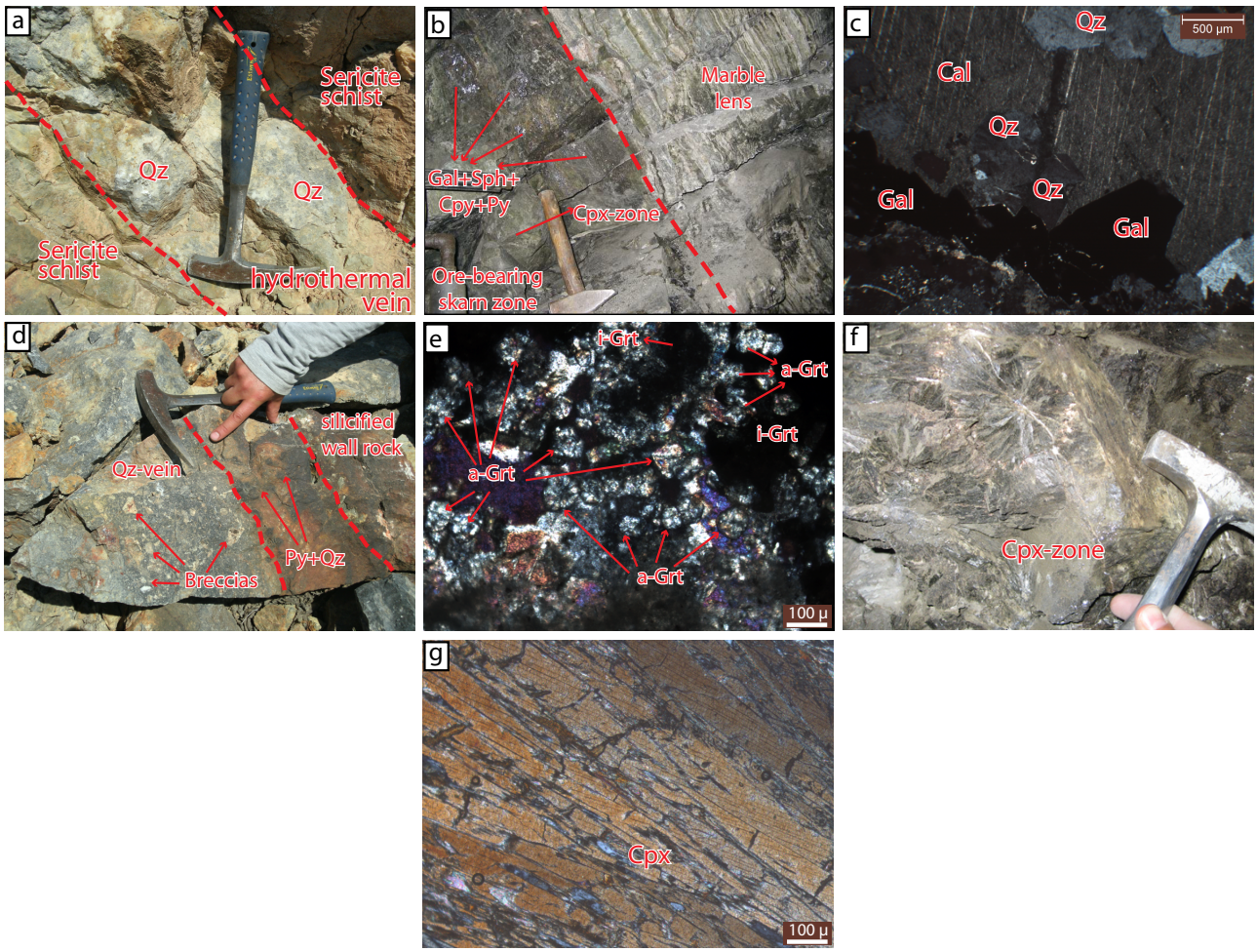


Figure 4. a. Ore-bearing quartz vein in the metadiabase (Arapuçandere deposit), b. marble lens and skarn zone in the Handeresi adit, c. hydrothermal vein including ore minerals and euhedral quartz and calcite (XPL), d. silicified wall rock and hydrothermal quartz vein including breccias of this wall rock (Kurttaşı mineralization), e. fine-medium-grained anisotropic garnets in the alteration zones, f. clinopyroxene zone in the Handeresi adit, g. microphotograph of the johannsennite minerals (XPL). (*Abbreviations: a-Grt: anisotropic garnet, Cal: calcite, Cpx: clinopyroxene, Cpy: chalcopyrite, Gal: galena, i-Grt: isotropic garnet, Py: pyrite, Qz: quartz, Sph: sphalerite.*)

4.4.2. Pb-Zn skarn mineralizations

The main alteration minerals are garnet, pyroxene, amphibole, chlorite, and epidote. The ore minerals that can be identified in polished thin sections include galena and semiopaque sphalerite. Quartz and calcite gangues and late-stage barren quartz and calcite veins are also observed. The euhedral and subhedral garnets are both isotropic (andradite) and anisotropic (grossular) (Figure 4e). Two different types of isotropic garnet were also determined as colorless and green colored. Garnets of different grain sizes were formed in the quartz and calcite gangue. Pyroxenes, which are generally in johannsenite-hedenbergite composition (Akıska et al. 2013; Akıska 2020), are observed on a mesoscopic scale in the Handeresi and Alandere regions (Figure 4f). These types of pyroxenes, which are mostly observed as rods, radial, and prismatic (Figure 4g), are fan-shaped. Some pyroxenes are partly carbonatized and chloritized. Actinolite-tremolite are seen on a mesoscopic scale in the Çulfa Çukuru area. The gaps between these minerals were filled with quartz and calcite. Ore minerals (especially galena and sphalerite) accompany radial masses of actinolite and tremolite. An observation of the actinolite-tremolite relicts in radial carbonate minerals in some thin sections indicates that they are probably carbonatized. Epidote, which is fine-grained and euhedral-subhedral, is rare in alteration zones.

5. Geochemistry

The ore-bearing and wall rocks were analyzed for major oxides (Table 2, 3), trace (Table 4), and rare earth elements (Table 5).

Table 2. Major oxide values of ore-bearing skarns and the wall rocks of the Pb-Zn deposits in the Sakarya fragment of the Biga Peninsula.

	SiO2	Al2O3	Fe2O3	MgO	CaO	Na2O	K2O	TiO2	P2O5	MnO	Cr2O3	LOI	Sum
	%	%	%	%	%	%	%	%	%	%	%	%	%
CC07_2_27	0.78	0.15	0.27	0.3	54.64	<0.01	0.03	0.01	<0.01	0.05	<0.002	43.7	99.96
DD13-04	0.55	0.08	0.16	0.69	54.5	0.01	0.04	<0.01	<0.01	<0.01	<0.002	43.8	99.87
SAM13-04A	0.82	0.18	0.21	0.22	55.09	0.02	0.03	0.01	0.02	0.02	<0.002	43.3	99.93
SARY13-02	0.06	0.01	0.07	0.47	55.82	<0.01	<0.01	<0.01	<0.01	0.02	<0.002	43.5	99.95
AD13-07	1.66	0.4	0.33	0.95	53.75	0.02	<0.01	0.02	0.02	0.17	<0.002	42.6	99.92
AU13-09	1.12	0.35	0.56	3.08	51.33	0.02	0.04	0.02	0.01	0.03	0.002	43.4	99.92
DD13-02A	1.69	0.33	0.24	2.09	52.7	0.02	0.04	0.01	<0.01	0.03	<0.002	42.8	99.91
SAM13-06A	1.79	0.3	0.4	0.23	54.27	<0.01	0.01	0.03	0.05	0.13	<0.002	42.7	99.92
KA13-01	0.36	0.08	0.17	5.47	49.4	0.03	0.04	<0.01	<0.01	0.01	<0.002	44.3	99.86
CC07_2_26	5.64	0.67	1.29	0.4	49.49	0.01	0.06	0.03	<0.01	3.89	<0.002	38.4	99.85
CO13-02	64.26	14.98	5.42	2.19	4.36	3.25	3.71	0.57	0.17	0.1	0.004	0.7	99.73
CO13-03	63.43	15.51	5.15	2.32	4.51	3.42	3.58	0.58	0.19	0.09	0.003	0.9	99.7
CO13-04	62.78	15.76	5.3	2.55	4.83	3.33	3.58	0.64	0.2	0.1	0.003	0.6	99.67
YO13-01	63.34	15.7	5.43	2.3	4.26	3.35	3.87	0.57	0.18	0.11	0.002	0.6	99.7
YO13-02	64.58	15.74	4.54	2.08	3.96	3.37	3.91	0.54	0.16	0.09	<0.002	0.7	99.7
CC07_2_10	62.55	15.97	5.27	3.05	3.38	2.85	2.49	0.53	0.14	0.11	0.020	3.4	99.79
AU13-10	59.97	15.35	5.52	1.86	4.54	2.73	3.78	0.6	0.22	0.08	<0.002	5.1	99.72
CC07_2_28	59.82	17.35	4.78	1.14	4.63	3.16	3.34	0.55	0.18	0.09	0.002	4.6	99.66
KAL-12	59.13	16.85	6.53	3.05	2.96	3.3	1.6	0.64	0.24	0.15	0.013	5.3	99.73
KAL-13	68.39	14.33	4.71	1.42	0.33	3	3.38	0.41	0.08	0.03	0.02	3.8	99.86
KAL-16	59.76	15.43	6.44	2.92	5.56	3.24	3.53	0.67	0.19	0.07	0.011	1.8	99.65
KS13-01	67.48	14.84	3.99	1.11	3.16	3.15	3.63	0.57	0.21	0.03	<0.002	1.6	99.76
KS13-02	58.19	17.41	6.48	1.52	4.44	3.24	3.07	0.76	0.4	0.07	<0.002	4.1	99.7
KS13-03	62.9	17.55	4.13	0.51	2.55	3.05	3.94	0.65	0.26	0.01	<0.002	4.2	99.75
CAT10-04B	58.81	16.36	6.45	2.19	5.41	3.41	3	0.68	0.21	0.1	0.007	3	99.66
CC07_2_29	52.36	13.90	5.33	1.97	9.12	2.88	1.19	0.50	0.17	0.27	<0.002	12.0	99.73
CC07_2_32	46.84	17.47	8.05	5.22	7.26	1.39	1.87	0.81	0.17	0.17	0.005	10.5	99.69
CC07_12	66.83	15.58	6.08	1.59	0.4	0.68	3.14	0.56	0.11	0.09	0.01	4.8	99.82
ASA13-02	58.14	13.56	10.63	4.33	1.79	0.89	1.92	0.99	0.25	0.44	0.012	6.8	99.77
CC07_2_17	70.78	15.92	2.71	1.08	0.11	1.3	3.56	0.52	0.04	0.02	0.01	3.8	99.85
GUM13-03	78.86	11.53	1.75	0.5	0.16	2.08	2.4	0.27	0.04	<0.01	0.004	2.3	99.92
MEN14	64.65	16.21	5.83	2.14	0.54	1.06	4.15	0.87	0.13	0.09	0.012	4.1	99.81
SAM13-02	64.64	15.5	5.74	1.49	2.74	2.07	2.98	0.81	0.09	0.09	0.01	3.6	99.81
SK13-01	72.82	10.75	3.22	1.04	3.7	1.98	1.85	0.34	0.09	0.04	0.006	4.1	99.9
YY13-01	61.86	16	6.43	2.42	2.24	1.43	3.69	0.72	0.12	0.15	0.013	4.7	99.82
ALD13-01	52.2	11.83	6.83	8.47	11.33	1.71	2.03	0.63	0.09	0.16	0.104	4.3	99.74
CO13-05	68.37	15.21	4.21	1.17	3.15	2.33	3.43	0.43	0.06	0.06	0.003	1.4	99.82
SS13-01	73.81	13.99	2.67	0.71	0.79	1.94	2.88	0.36	0.05	0.02	0.007	2.7	99.88
CC07_2_9	65.66	11.64	4.94	0.66	2.53	0.02	1.43	0.12	0.10	1.65	0.008	8.8	97.57
CAT10-02	78.04	10.29	2.74	0.88	1.54	2.45	1.89	0.24	0.06	0.06	0.007	1.7	99.85
CAT10-09A	66.14	13.68	7.53	1.89	0.42	0.26	3.47	1.14	0.23	0.09	0.009	4.9	99.82

Table 2. (Continued)

	SiO2	Al2O3	Fe2O3	MgO	CaO	Na2O	K2O	TiO2	P2O5	MnO	Cr2O3	LOI	Sum
	%	%	%	%	%	%	%	%	%	%	%	%	%
CC07_2_18	90.44	4.56	1.06	0.1	0.06	0.03	1.86	0.04	0.02	<0.01	<0.002	1.7	99.85
CC07_2_30	79.85	9.94	2.65	0.47	0.16	0.09	4.19	0.23	0.03	0.01	0.002	2.3	99.91
AD13-08	74.13	11.11	3.19	0.72	0.04	0.14	8.12	0.32	0.05	0.06	0.003	1.8	99.71
SO13-01	75.61	12.8	1.71	0.6	0.44	3.15	3.35	0.23	0.02	0.01	0.004	2	99.9
CC07_2_23	48.64	4.86	11.57	2.10	11.57	0.01	0.06	0.02	<0.01	7.93	<0.002	10.2	96.99
SAM13-03	54.34	1.09	10.42	3.18	13.41	0.06	<0.01	0.07	0.03	8.73	<0.002	4.4	95.68
CC07_2_36	45.37	0.57	13.15	5.13	18.11	0.09	0.02	0.03	0.04	7.95	<0.002	2.9	93.38
GUM13-07	50.78	0.32	12.15	1.88	12.95	0.05	0.02	<0.01	<0.01	13.97	<0.002	5.9	97.99
AD13-03	40.71	0.86	21.87	0.67	22.92	0.01	0.04	0.01	<0.01	6.64	0.005	3.4	97.14
AD13-04	48.78	0.97	8.15	2.66	17.71	0.03	0.02	0.05	<0.01	11.25	<0.002	2.6	92.24
CD13-01	50.87	0.23	10.42	2.60	15.77	0.03	0.03	<0.01	<0.01	11.62	<0.002	3.1	94.67
CC07_2_7	51.81	0.92	38.39	0.01	0.04	<0.01	0.08	0.04	0.05	0.01	0.003	6.7	98.10

Table 3. The major oxides of volcanic rocks that are normalized to 100% on a volatile-free basis.

	SiO2	Al2O3	Fe2O3	MgO	CaO	Na2O	K2O	TiO2	P2O5	MnO	Cr2O3	LOI	Sum
	%	%	%	%	%	%	%	%	%	%	%	%	%
AU13-10*	63.38	16.22	5.83	1.97	4.80	2.89	3.99	0.63	0.23	0.08	<0.002	-	100
CC07_2_2*8	62.93	18.25	5.03	1.20	4.87	3.32	3.51	0.58	0.19	0.09	0.002	-	100
KAL-12*	62.62	17.84	6.92	3.23	3.13	3.49	1.69	0.68	0.25	0.16	0.014	-	100
KAL-13*	71.20	14.92	4.90	1.48	0.34	3.12	3.52	0.43	0.08	0.03	0.021	-	100
KAL-16*	61.07	15.77	6.58	2.98	5.68	3.31	3.61	0.68	0.19	0.07	0.011	-	100
KS13-01*	68.74	15.12	4.06	1.13	3.22	3.21	3.70	0.58	0.21	0.03	<0.002	-	100
KS13-02*	60.87	18.21	6.78	1.59	4.64	3.39	3.21	0.79	0.42	0.07	<0.002	-	100
KS13-03*	65.83	18.37	4.32	0.53	2.67	3.19	4.12	0.68	0.27	0.01	<0.002	-	100
CAT10-04B*	60.84	16.93	6.67	2.27	5.60	3.53	3.10	0.70	0.22	0.10	0.007	-	100
CC07_2_29*	59.68	15.84	6.08	2.25	10.40	3.28	1.36	0.57	0.19	0.31	0.002	-	100
CC07_2_32*	52.52	19.59	9.03	5.85	8.14	1.56	2.10	0.91	0.19	0.19	0.006	-	100
CC07_12*	70.33	16.40	6.40	1.67	0.42	0.72	3.30	0.59	0.12	0.09	0.011	-	100

Pb-Zn skarns in the study areas are mostly distal type and low-temperature skarns (Akıska, et al. 2013; Akıska, 2020; Çiçek et al., 2021; Demirela and Akıska, 2022). Physicochemical conditions indicate that these skarns and hydrothermal Pb-Zn deposits were formed in similar time intervals and with similar fluids derived from the same magmatic/hydrothermal sources (e.g., Örgün et al., 2005; Bozkaya et al., 2008; Akıska et al., 2013; Bozkaya and Banks, 2015). In addition, the wall rocks are similar in both types of Pb-Zn mineralization (skarn and hydrothermal). For this reason, all mineralizations were evaluated together in the geochemical interpretation of the wall rocks.

5.1. Major oxide composition of ore and wall rocks

Analyses were made on the samples of the Oligo-Miocene calc-alkaline Yenice, Eybek, and Sarıoluk plutons outcropping in the Sakarya region of the Biga Peninsula. The obtained results are plotted on the granodiorite area of the total alkali versus silica (TAS) diagram (Middlemost, 1994) (Figure 5a). Samples of the Hallaçlar volcanics mostly fall into dacite, andesite, trachyandesite, and basaltic andesite areas, although one sample is a basalt and another sample is a basaltic andesite (Le Bas et al., 1986) (Figure 5b). The metasandstones are evaluated in Herron's (1988) terrigenous sandstones and shales

Table 4. Trace element values of ore-bearing skarns and the wall rocks of the Pb-Zn deposits in the Sakarya fragment of the Biga Peninsula.

	Ba	Be	Co	Cs	Ga	Hf	Nb	Rb	Sn	Sr	Ta	Th	U	V	W
	ppm	ppm	ppm	ppm	ppm	ppm	ppm	ppm	ppm	ppm	ppm	ppm	ppm	ppm	ppm
CC07_2_27	12	<1	<0.2	0.1	<0.5	<0.1	<0.1	1.7	<1	150	<0.1	<0.2	1.1	8	0.7
DD13-04	6	<1	<0.2	0.1	<0.5	<0.1	<0.1	1.1	<1	910	<0.1	<0.2	0.6	<8	<0.5
SAM13-04A	9	<1	<0.2	<0.1	<0.5	<0.1	0.2	1.2	<1	387	<0.1	<0.2	0.2	<8	<0.5
SARY13-02	7	<1	<0.2	<0.1	<0.5	<0.1	<0.1	<0.1	<1	301	<0.1	<0.2	0.4	<8	<0.5
AD13-07	27	<1	0.6	<0.1	<0.5	0.2	0.5	0.3	<1	413	<0.1	0.2	0.3	<8	0.6
AU13-09	13	<1	0.6	0.3	<0.5	0.1	0.2	2.8	<1	165	<0.1	<0.2	<0.1	11	<0.5
DD13-02A	13	<1	0.3	<0.1	<0.5	0.1	0.2	0.9	<1	342	<0.1	<0.2	0.4	<8	<0.5
SAM13-06A	4	<1	1.1	0.2	<0.5	0.1	0.7	1	<1	294	<0.1	0.7	0.1	<8	0.7
KA13-01	18	2	<0.2	<0.1	<0.5	<0.1	<0.1	0.8	<1	296	<0.1	<0.2	<0.1	<8	<0.5
CC07_2_26	8	2	<0.2	0.8	4.4	<0.1	<0.1	3.9	<1	174	<0.1	<0.2	0.5	23	1.2
CO13-02	831	5	9.6	6.1	14.4	5	14.6	149	2	525	1.3	53.2	18.6	113	1.1
CO13-03	990	2	10.7	7.3	17.2	4.8	14.3	153	2	593	1.3	24.4	8.5	106	1.6
CO13-04	1179	3	11.5	5.5	15.9	5	15.3	134	1	654	1	37.3	10.5	115	1.6
YO13-01	1043	2	12.3	6.3	15.2	4.9	15.2	147	2	547	1.7	37	12.9	110	3.5
YO13-02	1177	5	10.9	6.2	14.1	4.5	13.3	150	1	556	1.2	28.6	8.7	89	3.8
CC07_2_10	615	3	37.1	9.4	19.0	3.8	9.9	110.3	4	314.2	0.8	8.7	3.1	92	126.7
AU13-10	1027	4	8.4	6.1	16.4	4.5	13.6	139	1	523	1	29.5	9	108	2
CC07_2_28	1292	2	12.1	3.2	18	5.1	12.1	115	2	821	1	28.2	7.5	99	1.8
KAL-12	637	4	14.8	3.5	17	3.8	7	53.3	1	629	0.4	15.1	4.7	145	1.4
KAL-13	658	2	1.6	2.9	16.5	3.2	8.4	103	4	150	0.9	18.4	5.2	72	1.5
KAL-16	1221	<1	18.3	5.5	14.8	4.5	11.9	121	4	769	1.1	33.6	7.9	114	1.9
KS13-01	958	1	6.5	6.2	13.1	3.9	12.4	112	1	530	1	29.3	5.2	93	1.5
KS13-02	1112	3	12.8	0.7	15.6	4.4	12.7	60.9	1	596	1	29.3	4.7	79	1.4
KS13-03	1029	1	20.3	4.3	14.1	4.5	11.8	123	1	500	0.9	24.7	6.4	88	3.4
CAT10-04B	1236	2	18.6	3.4	15.3	3.9	10.6	95.6	<1	724	0.9	20	6.4	140	2.2
CC07_2_29	402	2	13.2	3.7	15.7	3.0	9.4	58.0	2	407.7	0.8	16.8	5.3	91	28.7
CC07_2_32	503	1	26.8	15.0	17.4	3.8	6.8	134.9	1	252.6	0.4	7.7	2.5	199	18.0
CC07_12	696	4	16.3	11.5	18.8	5.1	9.2	139	3	52.5	0.7	11.7	2.6	103	2
ASA13-02	351	2	24.5	2.6	16.4	3	4.2	95.9	1	76	0.4	4.3	3.2	306	1.3
CC07_2_17	511	4	6.5	11.2	17.6	6	12.7	173	5	42.9	1	14.2	4.4	77	2.4
GUM13-03	347	1	2.1	5.1	12.4	4	8.4	107	4	66.5	0.9	11.3	3.2	36	1.8
MEN14	652	<1	12.6	5.7	18.2	5.8	12.6	149	3	78.1	1	12.4	2.6	108	4.7
SAM13-02	581	<1	12.3	2.5	17.4	6.2	12.1	96.6	3	191	1	14.2	3.5	109	2.6
SK13-01	274	3	5.2	1.4	12	3.4	7.9	78.1	3	149	0.6	12	2.1	51	<0.5
YY13-01	508	1	13.1	6.1	15.4	4.8	10.8	127	2	111	1	11.2	2.1	120	2.8
ALD13-01	266	3	34.7	1	12.7	2.8	8.2	53.5	1	306	0.5	6.7	1.6	130	<0.5
CO13-05	683	2	4.7	6	12.7	5	10.5	101	<1	165	0.7	15.3	3	63	0.9
SS13-01	450	3	4.3	2.5	14.4	6.1	10.9	100	5	86.8	1.1	16.7	3.5	40	1.9
CC07_2_9	326	2	18.6	32.6	15.6	1.3	2.6	126.2	3	14.6	0.2	8.7	2.4	90	96.0
CAT10-02	301	1	47.1	1.9	9.7	4.8	8.0	72.0	3	120.5	0.8	12.6	3.5	23	352.6
CAT10-09A	390	2	37.4	16.3	20.0	7.5	28.9	159.3	3	30.2	1.8	10.2	2.2	130	106.1

Table 4. (Continued)

	Ba	Be	Co	Cs	Ga	Hf	Nb	Rb	Sn	Sr	Ta	Th	U	V	W
	ppm	ppm	ppm	ppm	ppm	ppm	ppm	ppm	ppm	ppm	ppm	ppm	ppm	ppm	ppm
CC07_2_18	984	2	0.3	8.9	4.6	1.1	3	79.6	<1	20.8	0.4	5.3	0.8	8	1.1
CC07_2_30	555	2	1	7.8	9.8	2.4	5.3	170	1	27.9	0.4	7.1	1.1	28	2.8
AD13-08	1509	<1	37.5	5.4	10.5	4.4	8.7	300.6	2	138.3	0.8	7.6	1.3	37	285.7
SO13-01	589	<1	1.5	3.1	9.9	2.7	3.9	106	1	58.8	0.3	6.5	1.2	29	0.8
CC07_2_23	61	24	43.2	48.2	11.2	0.3	0.4	15.5	<1	57.9	<0.1	0.4	0.9	29	274.6
SAM13-03	32	6	39.4	6.0	7.1	0.2	0.7	1.8	<1	19.4	<0.1	0.5	0.5	26	84.4
CC07_2_36	5	9	20.0	4.3	7.7	0.2	0.9	1.1	<1	30.4	<0.1	0.5	0.9	21	52.5
GUM13-07	2	5	7.1	6.6	9.8	<0.1	0.2	1.9	<1	77.1	<0.1	<0.2	1.5	13	47.6
AD13-03	4	3	31.1	7.4	8.2	0.1	0.3	5.5	<1	15.0	<0.1	0.2	1.2	15	216.2
AD13-04	4	3	16.2	4.3	9.0	0.2	0.7	1.6	<1	20.2	<0.1	0.4	0.4	15	58.9
CD13-01	190	10	23.6	5.9	8.8	<0.1	<0.1	1.6	<1	84.8	<0.1	<0.2	0.2	<8	128.1
CC07_2_7	19	<1	15.6	1.7	4.5	0.3	0.7	6.7	<1	2.5	<0.1	0.5	2.2	28	126.1

	Zr	**Mo**	**Cu**	**Pb**	**Zn**	**Ni**	**As**	**Cd**	**Sb**	**Bi**	**Ag**	**Au**	**Hg**	**Tl**	**Se**
	ppm	**ppm**	**ppm**	**ppm**	**ppm**	**ppm**	**ppm**	**ppm**	**ppm**	**ppm**	**ppm**	**ppb**	**ppm**	**ppm**	**ppm**
CC07_2_27	2.9	0.4	1.5	4	44	2.6	6.2	<0.1	0.7	<0.1	<0.1	1.6	<0.01	<0.1	<0.5
DD13-04	1.2	0.2	1	1	4	2	1.7	<0.1	<0.1	<0.1	<0.1	<0.5	<0.01	<0.1	<0.5
SAM13-04A	2.6	<0.1	0.9	2.5	6	1	0.8	<0.1	<0.1	<0.1	<0.1	0.7	<0.01	<0.1	<0.5
SARY13-02	0.4	<0.1	0.7	2.2	9	2.7	0.9	0.1	<0.1	<0.1	<0.1	0.6	<0.01	<0.1	<0.5
AD13-07	6	<0.1	1	3.5	19	3	0.6	0.3	<0.1	<0.1	<0.1	0.8	<0.01	<0.1	<0.5
AU13-09	4.1	0.1	3.1	4.3	18	4.2	4.8	0.7	0.2	<0.1	<0.1	<0.5	0.01	<0.1	<0.5
DD13-02A	3.3	0.1	1	2.7	5	2.6	<0.5	<0.1	<0.1	<0.1	<0.1	<0.5	<0.01	<0.1	<0.5
SAM13-06A	7.6	0.1	5.2	18.2	150	2.3	0.6	0.2	<0.1	<0.1	<0.1	0.7	<0.01	<0.1	<0.5
KA13-01	3.2	<0.1	0.8	0.7	6	1.4	0.8	0.1	<0.1	<0.1	<0.1	<0.5	<0.01	<0.1	<0.5
CC07_2_26	5.5	0.3	1.6	234.7	408	2.5	43.7	1.9	0.8	<0.1	0.1	11.7	0.02	<0.1	<0.5
CO13-02	161	0.5	4.9	10.5	27	5.7	5.2	<0.1	0.2	<0.1	<0.1	0.6	<0.01	0.3	<0.5
CO13-03	165	0.7	8.7	8.8	25	5.2	2.2	<0.1	<0.1	<0.1	<0.1	<0.5	<0.01	0.3	<0.5
CO13-04	185	0.2	7.2	6.2	28	5.1	1.2	<0.1	<0.1	<0.1	<0.1	<0.5	<0.01	0.4	<0.5
YO13-01	173	1.1	28.1	31.8	39	6.6	5.3	0.2	0.4	0.2	<0.1	<0.5	<0.01	0.3	<0.5
YO13-02	164	1.2	20.5	29.1	37	7.4	4.6	0.1	0.2	0.2	<0.1	<0.5	<0.01	0.4	<0.5
CC07_2_10	121.7	<0.1	5.1	17.1	52	35.3	3.7	<0.1	0.5	0.1	<0.1	3.7	<0.01	0.1	<0.5
AU13-10	157	1	27.2	13.7	53	7	<0.5	0.3	<0.1	<0.1	<0.1	0.9	<0.01	<0.1	<0.5
CC07_2_28	202	0.2	15.7	15.3	58	7.9	5.2	<0.1	0.1	0.3	<0.1	<0.5	0.04	<0.1	<0.5
KAL-12	148	0.2	10.9	17.9	59	7.3	2.6	0.2	<0.1	0.1	<0.1	<0.5	0.06	<0.1	<0.5
KAL-13	107	0.5	10.6	6.6	31	12	1.2	<0.1	<0.1	0.4	<0.1	<0.5	<0.01	<0.1	0.6
KAL-16	169	0.2	17.1	3.4	36	6.8	5.3	<0.1	0.2	<0.1	<0.1	<0.5	<0.01	<0.1	<0.5
KS13-01	139	0.4	4.8	5.7	19	5.5	1.9	<0.1	0.3	<0.1	<0.1	1	<0.01	0.2	<0.5
KS13-02	162	0.3	25.2	5.3	27	5.4	1.6	<0.1	0.1	<0.1	<0.1	1.2	0.02	<0.1	<0.5
KS13-03	160	0.4	30.1	12.7	37	9.1	5.9	0.2	0.2	4.1	<0.1	<0.5	0.01	0.7	<0.5
CAT10-04B	162	0.6	31.8	6.3	55	11.8	2	<0.1	0.4	<0.1	<0.1	<0.5	0.01	<0.1	<0.5
CC07_2_29	141.2	0.3	1.8	61.6	69	1.7	3.3	0.3	<0.1	0.2	<0.1	1.0	<0.01	<0.1	<0.5
CC07_2_32	155.4	<0.1	2.4	19.4	102	5.4	17.9	0.2	<0.1	<0.1	<0.1	0.5	<0.01	<0.1	<0.5

Table 4. (Continued)

	Zr	Mo	Cu	Pb	Zn	Ni	As	Cd	Sb	Bi	Ag	Au	Hg	Tl	Se
	ppm	ppm	ppm	ppm	ppm	ppm	ppm	ppm	ppm	ppm	ppm	ppb	ppm	ppm	ppm
CC07_12	174	<0.1	18.3	16	102	39.5	0.7	0.1	<0.1	<0.1	<0.1	<0.5	0.02	0.1	<0.5
ASA13-02	109	4.2	56.2	14.2	245	81.4	6	2.1	0.1	0.4	<0.1	2.1	0.02	<0.1	<0.5
CC07_2_17	210	0.3	19.6	6.6	15	21.7	12.9	<0.1	0.6	0.3	<0.1	<0.5	0.07	0.3	<0.5
GUM13-03	136	0.1	18.1	16.1	25	13.5	3.1	<0.1	0.1	0.3	<0.1	<0.5	<0.01	<0.1	<0.5
MEN14	220	0.5	6.8	5.3	65	35.7	657	<0.1	1.4	0.2	<0.1	1.4	<0.01	<0.1	<0.5
SAM13-02	240	0.4	22.2	10.8	76	32.6	11	0.7	0.5	0.2	<0.1	<0.5	<0.01	<0.1	<0.5
SK13-01	113	0.4	18.2	20.1	50	22.9	1.9	<0.1	<0.1	0.6	<0.1	0.5	<0.01	<0.1	<0.5
YY13-01	171	2.4	29.4	14.5	88	50.6	36.7	0.1	0.1	0.3	<0.1	0.6	0.02	<0.1	<0.5
ALD13-01	106	0.6	37.2	7	32	220	<0.5	<0.1	<0.1	0.1	0.1	1.1	<0.01	<0.1	<0.5
CO13-05	180	0.4	13.6	16.3	39	19.5	5.6	<0.1	0.2	<0.1	<0.1	<0.5	<0.01	0.4	<0.5
SS13-01	209	0.6	9.2	12.4	57	20.5	5.1	<0.1	<0.1	0.4	<0.1	<0.5	0.14	<0.1	<0.5
CC07_2_9	53.9	1.8	171.1	>10,000.0	6976	39.0	191.4	32.6	2.5	0.8	4.2	79.9	0.32	2.6	<0.5
CAT10-02	187.4	0.1	4.1	44.5	93	22.5	12.1	0.4	0.5	0.2	<0.1	12.7	*	<0.1	<0.5
CAT10-09A	328.6	0.2	60.4	8.7	59	131.5	49.3	<0.1	0.4	0.3	<0.1	2.2	<0.01	0.5	0.8
CC07_2_18	28.1	1.5	22.2	346.2	62	1.3	171	<0.1	7.2	0.1	0.7	31.3	0.05	<0.1	<0.5
CC07_2_30	90.8	0.5	10.3	10.1	28	2.7	197	<0.1	4.6	<0.1	0.1	8.3	0.08	0.1	<0.5
AD13-08	162.5	0.8	6.6	42.9	234	3.2	50.2	0.7	1.0	<0.1	0.8	11.7	*	0.1	<0.5
SO13-01	95.2	0.2	6.4	8	24	4.3	8.8	<0.1	0.3	0.2	<0.1	1.4	0.02	0.1	<0.5
CC07_2_23	8.5	0.2	5.5	>10,000.0	5688	6.8	234.4	28.3	15.8	0.1	7.5	140.0	0.04	0.9	2.5
SAM13-03	9.8	0.1	54.2	>10,000.0	>10,000	3.6	155.4	138.1	13.1	<0.1	5.3	48.1	0.04	0.2	4.3
CC07_2_36	7.9	0.1	120.6	>10,000.0	>10,000	2.0	106.4	235.1	17.6	0.3	9.6	126.2	0.03	<0.1	26.9
GUM13-07	3.2	0.2	4.0	2886.0	>10,000	0.6	116.6	70.2	29.3	<0.1	1.0	19.1	<0.01	<0.1	<0.5
AD13-03	4.2	0.3	90.1	>10,000.0	>10,000	2.5	648.9	86.1	10.3	<0.1	7.6	90.5	0.03	<0.1	2.1
AD13-04	10.7	0.1	13.8	>10,000.0	>10,000	2.6	60.3	240.8	12.5	<0.1	7.5	31.9	0.03	0.2	4.2
CD13-01	1.1	0.2	55.4	>10,000.0	>10,000	0.4	145.5	175.4	15.0	<0.1	6.7	27.0	0.01	0.1	3.0
CC07_2_7	11.2	1.9	289.1	>10,000.0	2945	5.7	543.1	3.0	22.4	0.1	3.5	543.8	0.04	0.3	3.1

classification diagram (Figure 5c). The metasandstones are plotted mostly in the arkose area, and one sample each in the wacke, subarkose and litharenite areas. Petrographic observations also support the analysis results.

Major oxide compositions of the wall rocks show a consistent distribution within their rock groups (Table 2). Slight increases in MgO, MnO, and Fe_2O_3 values also indicate possible initial element enrichment in the wall rocks. CaO enrichment of the wall rocks, with the exception of marble, may be due to the calcite veinlets. However, enrichments in base metal and Ni values together with CaO also indicate possible ore interactions. Similar to the wall rocks, there is an enrichment in MgO, MnO, and Fe_2O_3 values in the ore samples. TiO_2 contents of schist, metasandstone and igneous rocks are above 0.5 wt.%; however, they are included in the ore samples much lower ratios (<0.1 wt.%).

According to the major oxide results of carbonaceous occurrences, the fresh marble has high CaO (54.5–55.82 wt.%) and loss-on-ignition (LOI) (43.3–43.8 wt.%) values with the other oxide values being negligible. SiO_2 (1.12–1.79 wt.%), Fe_2O_3 (0.24–0.56 wt.%), MnO (0.03–0.17 wt.%), and MgO (0.23–3.08 wt.%) contents show increases in the ore zone. These values are much higher in ore calcite (SiO_2: 0.36–5.64 wt.%, Fe_2O_3: 0.17–1.29 wt.%, MnO: 0.01–3.89 wt.%, MgO: 0.4–5.47 wt.%). The concentrations of MnO and MgO in ore and ore calcite are inversely proportional.

5.2. Trace element composition of ore and wall rocks

Trace element concentrations of wall rocks were normalized to average reference rock trace element values

Table 5. Y+REE values of ore-bearing skarns and the wall rocks of the Pb-Zn deposits in the Sakarya fragment of the Biga Peninsula.

	Y	La	Ce	Pr	Nd	Sm	Eu	Gd	Tb	Dy	Ho	Er	Tm	Yb	Lu	ΣREE	$(Pr/Yb)_{cn}$	Ce/Ce*	Eu/Eu*	Y/Ho
	ppm	ppm	ppm	ppm	ppm	ppm	ppm	ppm	ppm	ppm	ppm	ppm	ppm	ppm	ppm					
CC07_2_27	1.6	1.2	2	0.2	0.8	0.09	0.05	0.16	0.03	0.12	0.04	0.12	0.02	0.09	0.02	4.93	3.69	0.91	1.34	40.00
DD13-04	3.6	2.5	2.3	0.5	2	0.44	0.13	0.5	0.08	0.43	0.09	0.25	0.02	0.18	0.02	9.42	4.67	0.47	0.90	40.00
SAM13-04A	5.3	3.6	1.9	0.5	1.7	0.34	0.11	0.59	0.07	0.45	0.1	0.28	0.04	0.27	0.04	9.94	2.92	0.31	0.79	53.00
SARY13-02	2.2	1.2	0.9	0.2	0.7	0.12	0.03	0.24	0.02	0.2	0.04	0.11	0.02	0.12	0.01	3.95	3.50	0.38	0.56	55.00
AD13-07	6	3.7	4	0.6	2.5	0.48	0.12	0.59	0.1	0.61	0.14	0.46	0.07	0.32	0.05	13.76	3.39	0.58	0.73	42.86
AU13-09	5.5	2.8	1.9	0.4	1.5	0.32	0.09	0.42	0.07	0.39	0.1	0.32	0.05	0.24	0.04	8.63	2.84	0.38	0.80	55.00
DD13-02A	1.7	3.1	4.6	0.5	1.9	0.35	0.26	0.43	0.06	0.25	0.05	0.18	0.02	0.1	0.02	11.79	8.23	0.82	2.18	34.00
SAM13-06A	9.5	6.5	8.7	1	4.2	0.78	0.12	0.98	0.14	0.93	0.21	0.57	0.08	0.5	0.07	24.79	3.54	0.73	0.45	45.24
KA13-01	1.9	1	1.3	0.2	0.5	0.1	0.03	0.16	0.03	0.13	0.04	0.08	0.01	0.11	0.01	3.66	2.55	0.70	0.77	47.50
CC07_2_26	1.6	2.9	3	0.4	1.5	0.29	0.13	0.24	0.05	0.2	0.04	0.06	0.02	0.06	0.02	8.94	12.54	0.57	1.57	40.00
CO13-02	24.5	53.8	102	11	37.6	6.53	1.21	5.67	0.8	4.31	0.84	2.22	0.39	2.85	0.4	229.33	6.51	0.96	0.63	
CO13-03	23.5	52.7	96	9.8	34.7	6.92	1.31	5.17	0.74	4.54	0.8	2.46	0.39	2.51	0.39	218.42	6.83	0.94	0.69	
CO13-04	25.4	49.5	96.9	10	36.9	6.77	1.43	5.82	0.84	4.36	0.95	2.56	0.35	2.48	0.37	219.45	7.21	0.98	0.73	
YO13-01	25.2	65.6	114	12	37.1	6.1	1.28	5.15	0.72	4.04	0.81	2.34	0.34	2.38	0.38	251.27	8.48	0.91	0.73	
YO13-02	18.2	46.8	78.8	8.1	26.9	4.82	1.19	4.21	0.56	3.3	0.61	1.81	0.28	1.84	0.32	179.58	7.74	0.89	0.84	
CC07_2_10	22.0	30.9	58.3	7.24	26.9	5.17	1.14	4.25	0.66	3.52	0.70	1.91	0.31	1.87	0.27	143.14	6.78	0.90	0.77	
AU13-10	21.3	52.3	96.8	10	36.1	6.04	1.32	5.01	0.7	3.67	0.76	2.33	0.33	2.22	0.33	217.99	7.95	0.95	0.76	
CC07_2_28	22.9	53.5	91.4	10	37.6	6.16	1.62	5.28	0.74	4.24	0.8	2.24	0.32	2.33	0.38	216.78	7.64	0.88	0.91	
KAL-12	29.5	38.8	67.3	8.7	35.2	7.07	1.79	6.5	0.95	5.69	1.04	3.11	0.43	2.8	0.46	179.85	5.44	0.84	0.85	
KAL-13	10.2	28.6	34.2	4.7	16	2.4	0.49	2.02	0.3	1.74	0.39	1.15	0.18	1.21	0.21	93.56	6.75	0.64	0.71	
KAL-16	23.8	57	110	12	42.8	7.07	1.5	5.74	0.79	4.34	0.83	2.19	0.33	2.26	0.36	247.06	8.94	0.97	0.75	
KS13-01	16	54.3	94	9.3	29.7	4.65	1.16	3.58	0.51	2.77	0.5	1.5	0.23	1.59	0.24	204.01	10.21	0.92	0.90	
KS13-02	25.7	56.1	96.8	11	37.7	6.37	1.5	5.3	0.78	4.09	0.85	2.36	0.36	2.44	0.4	226.40	8.14	0.87	0.82	
KS13-03	17.2	40.1	67.1	7.9	27.3	5.16	1.44	4.41	0.64	3.39	0.64	1.85	0.28	1.91	0.3	162.40	7.22	0.85	0.96	
CAT10-04B	19.9	47.6	79.7	8.8	32.6	5.95	1.44	4.78	0.64	3.44	0.66	2.04	0.3	1.83	0.29	190.04	8.39	0.87	0.85	
CC07_2_29	19.7	34.3	63.9	7.34	28.4	4.85	1.23	4.11	0.63	3.47	0.66	1.91	0.29	1.88	0.29	153.26	6.83	0.92	0.88	
CC07_2_32	22.8	17.4	36.7	4.52	19.8	4.15	1.11	4.31	0.72	4.08	0.85	2.44	0.38	2.47	0.38	99.31	3.20	0.97	0.85	
CC07_12	37.5	21.9	48.7	5.1	22.3	4.63	1.02	5.18	0.93	5.92	1.32	4.12	0.61	4.02	0.63	126.41	2.23	1.06	0.68	
ASA13-02	31.6	19.5	33.3	4.6	19.5	4.55	1.02	4.7	0.85	5.7	1.24	3.67	0.57	3.87	0.59	103.69	2.09	0.81	0.71	
CC07_2_17	40.7	49.1	48.5	13	53.6	9.66	1.43	8.34	1.23	6.59	1.45	4.13	0.55	3.65	0.53	201.71	6.21	0.45	0.51	
GUM13-03	17.7	14.6	26	2.8	11.1	2	0.34	2.29	0.43	2.74	0.65	1.93	0.3	2.07	0.34	67.63	2.40	0.91	0.52	
MEN14	21.7	37.6	72.4	8.7	30.3	5.75	0.98	4.96	0.74	4	0.78	2.09	0.32	2.1	0.35	171.07	7.25	0.92	0.59	
SAM13-02	26	41.3	77.5	9.2	31.6	5.81	1.13	5.13	0.78	4.61	0.94	2.73	0.44	2.77	0.41	184.30	5.78	0.91	0.66	
SK13-01	19.3	17.1	41.4	4.2	13.7	3.03	0.5	2.9	0.49	2.89	0.64	2.04	0.31	2.31	0.36	91.82	3.14	1.14	0.54	
YY13-01	30.1	22.5	43.4	5	19	4.05	0.9	4.24	0.8	5.12	1.11	3.05	0.45	2.92	0.45	113.02	3.01	0.94	0.70	
ALD13-01	17.7	22.2	40.3	4.6	18	3.45	0.8	3.4	0.57	3.13	0.74	2.1	0.32	2.03	0.31	101.98	3.99	0.90	0.75	
CO13-05	22	33.8	66.8	7.1	25.6	5.26	1.01	4.71	0.72	4.14	0.82	2.53	0.37	2.56	0.43	155.82	4.83	0.98	0.65	
SS13-01	22.7	21.6	30.7	5.1	17.4	3.63	0.55	3.23	0.56	3.41	0.71	2.28	0.37	2.49	0.38	92.37	3.56	0.68	0.51	
CC07_2_9	17.5	24.2	50.8	5.72	22.9	4.61	1.17	4.01	0.64	3.49	0.66	1.90	0.29	1.75	0.27	122.41	5.72	1.00	0.87	
CAT10-02	24.5	27.9	51.1	6.69	25.3	4.86	0.81	4.55	0.76	4.22	0.84	2.40	0.36	2.33	0.35	132.47	5.02	0.87	0.55	
CAT10-09A	32.8	34.3	69.9	8.79	35.5	6.58	1.28	5.86	1.00	5.63	1.17	3.36	0.54	3.39	0.50	177.80	4.54	0.94	0.66	
CC07_2_18	10.3	9	16	1.7	5.8	1.14	0.17	1.34	0.25	1.55	0.38	1.1	0.17	1.1	0.18	39.88	2.70	0.91	0.45	
CC07_2_30	7.6	14	25.5	3.2	10.9	1.98	0.3	1.65	0.27	1.44	0.3	0.93	0.14	0.96	0.14	61.70	5.82	0.88	0.53	
AD13-08	6.5	6.9	5.7	1.78	6.6	1.24	0.31	1.00	0.19	1.12	0.25	0.83	0.14	0.99	0.16	27.21	3.15	0.38	0.88	
SO13-01	10.1	19.1	34.1	3.9	13.4	2.24	0.6	1.89	0.31	1.65	0.37	0.98	0.15	1.03	0.15	79.86	6.61	0.90	0.93	
CC07_2_23	4.7	7.3	10.6	1.18	4.5	0.72	0.48	0.67	0.10	0.63	0.13	0.38	0.05	0.40	0.06	27.20	5.16	0.78	2.22	
SAM13-03	2.7	2.3	4.0	0.53	2.2	0.42	0.10	0.41	0.06	0.38	0.08	0.24	0.04	0.20	0.03	10.99	4.64	0.83	0.78	
CC07_2_36	8.3	3.1	2.4	0.65	2.8	0.57	0.09	0.70	0.11	0.67	0.15	0.48	0.07	0.39	0.07	12.25	2.92	0.38	0.46	
GUM13-07	1.0	0.8	1.2	0.15	0.6	0.10	0.03	0.11	0.02	0.14	0.03	0.06	0.01	0.08	0.01	3.34	3.28	0.77	0.93	
AD13-03	2.5	2.4	3.7	0.57	1.9	0.39	0.15	0.36	0.06	0.32	0.06	0.20	0.02	0.17	0.03	10.33	5.87	0.73	1.29	
AD13-04	5.3	2.2	3.1	0.49	2.3	0.40	0.07	0.45	0.08	0.52	0.13	0.42	0.06	0.37	0.05	10.64	2.32	0.68	0.54	
CD13-01	4.4	2.4	1.6	0.40	1.5	0.27	0.07	0.30	0.05	0.32	0.07	0.22	0.03	0.16	0.02	7.41	4.38	0.36	0.80	
CC07_2_7	3.3	1.7	1.4	0.49	2.1	0.51	0.13	0.52	0.09	0.50	0.10	0.30	0.05	0.30	0.04	8.23	2.86	0.36	0.82	

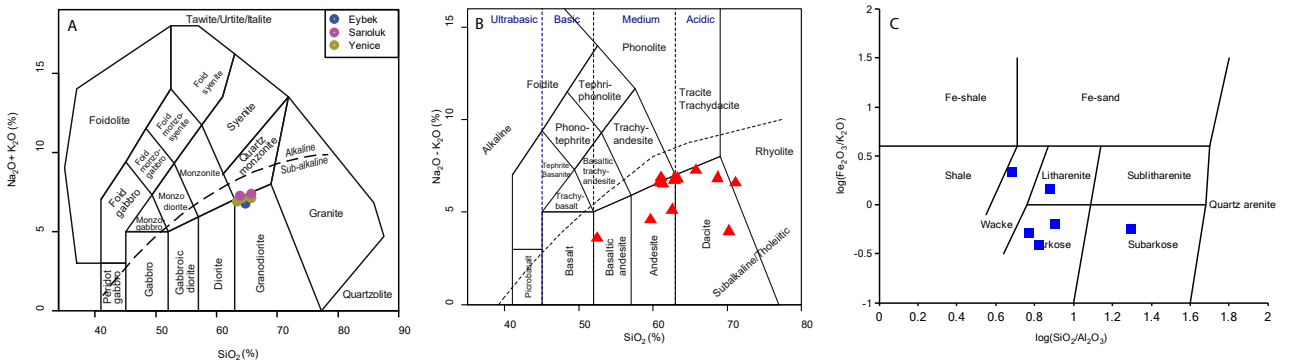


Figure 5. Evaluation of (a) the plutons in the SiO_2 vs. Na_2O+K_2O diagram (Middlemost, 1994), (b) the volcanics in the SiO_2 vs. Na_2O+K_2O diagram (the major oxide values of volcanic rocks normalized to 100% on a volatile-free basis in Table 3 are used) (Le Bas et al., 1986), and (c) the metasandstones in the Herron (1988)'s terrigenous sandstones and shales classification diagram.

Table 6. Reference rock trace element values.

Rock type (this study)	Reference rock	Elements	Reference
Plutonic rocks	Granitic rocks-low Ca	Ba, Be, Ga, Hf, Nb, Rb, Sr, Th, U, V, Zr, Y, Cu, Pb, Zn, As	Turekian and Wedepohl (1961)
Volcanic rocks	Andesite	Ba, Hf, Nb, Rb, Sr, Th, U, V, Zr, Y, Cu, Pb	Taylor (1969)
	Basaltic rocks	Be, Ga, Zn, As	Turekian and Wedepohl (1961)
Marble	Carbonate rocks	Ba, Rb, Sr, U, Zr, Y, Cu, Pb, Zn, As, Cd	Turekian and Wedepohl (1961)
Schist	Shale	Ba, Be, Ga, Hf, Nb, Rb, Sr, Th, U, V, Zr, Y, Cu, Pb, Zn, As, Sb	Turekian and Wedepohl (1961)
Metasandstone	Sandstones	Ba, Be, Ga, Hf, Nb, Rb, Sr, Th, U, V, Zr, Y, Cu, Pb, Zn, As, Cd, Sb, Ag, Au	Turekian and Wedepohl (1961)

(Turekian and Wedepohl, 1961; Taylor, 1969) (Table 6; Figure 6). Although small enrichments are seen in the Sr, Th, and U values in plutonic rocks (Figure 6a), they are generally similar to the reference rock values. Th and U values show enrichment of up to 10 times, while a few Cu values show depletion of up to 10 times (or more) in volcanic rocks (Figure 6b). While the Pb value of one sample (CC07_2_29) shows enrichment of up to 10 times, the As value of another sample (CC07_2_32) shows a similar enrichment (Figure 6b). The Ba, Rb, Sr, U, Zr, and Y values in the marble show slight decreases compared to the average values of the reference rocks (Figure 6c). However, minor enrichment is observed in ore-related elements (Cu, Pb, Zn, As, and Cd), although these values are relatively higher in one sample (CC07_2_26) (Figure 6c). In the spidergram obtained from the schists, it was determined that the samples (with the exception of a few) had almost the same pattern as the reference rock (Figure 6d). The ore-bearing graphite schist sample (CC07_2_9) is typical due to low Sr and high Cu, Pb, Zn, and As anomalies. The other sample (MEN14) has a high As anomaly. Negative Sb anomalies of up to 10 times were also detected in some samples (Figure 6d). Significant enrichments were determined in Nb, As and Sb in metasandstones compared to the average reference values. Increases in ore elements (Pb, Zn, Cu, Cd, and Ag) and decreases in Zr and Y values compared to the reference values are observed in a few samples (Figure 6e).

5.3. Rare earth element composition of ore and wall rocks

Chondrite- (Boynton, 1984) and ore-bearing skarn-normalized (average values of ore-bearing skarn samples) REE patterns of the wall rocks related to the Biga Pb-Zn mineralizations are seen in Figure 7. The ΣREE values of fresh marble, ore zone marble, and ore calcite are 3.95–9.94 ppm (avg: 7.06 ppm, standard deviation (SD): 3.06, n: 4), 8.63–24.79 ppm (avg: 14.74 ppm, SD: 7.02, n: 4), 3.66–8.94 ppm (avg: 6.30, SD: 3.73, n: 2), respectively. While the ΣREE values in fresh marble and ore calcite are low, they

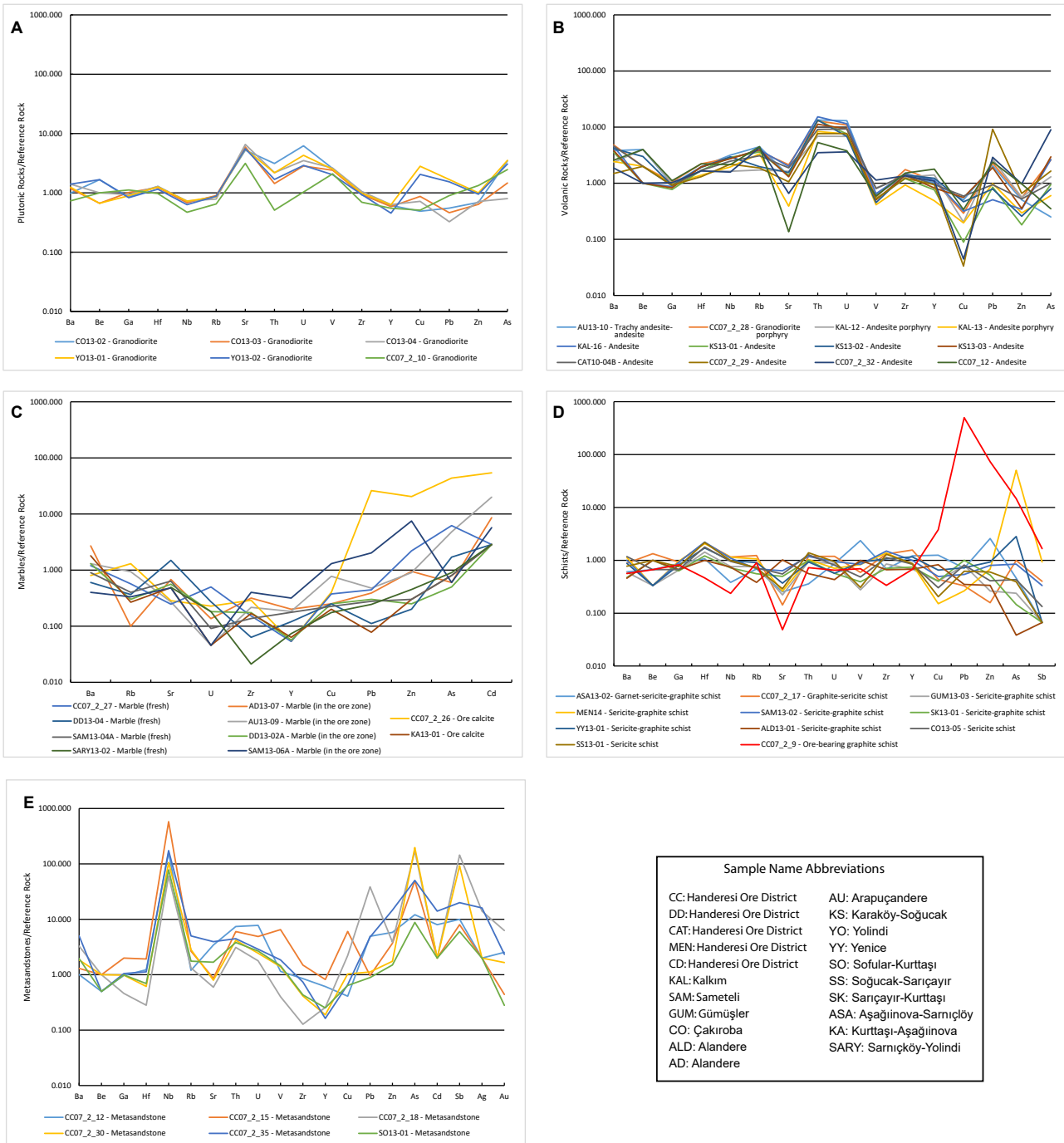


Figure 6. Trace element spider diagrams of the wall rocks normalized to reference rock values (Turekian and Wedepohl, 1961; Taylor, 1969).

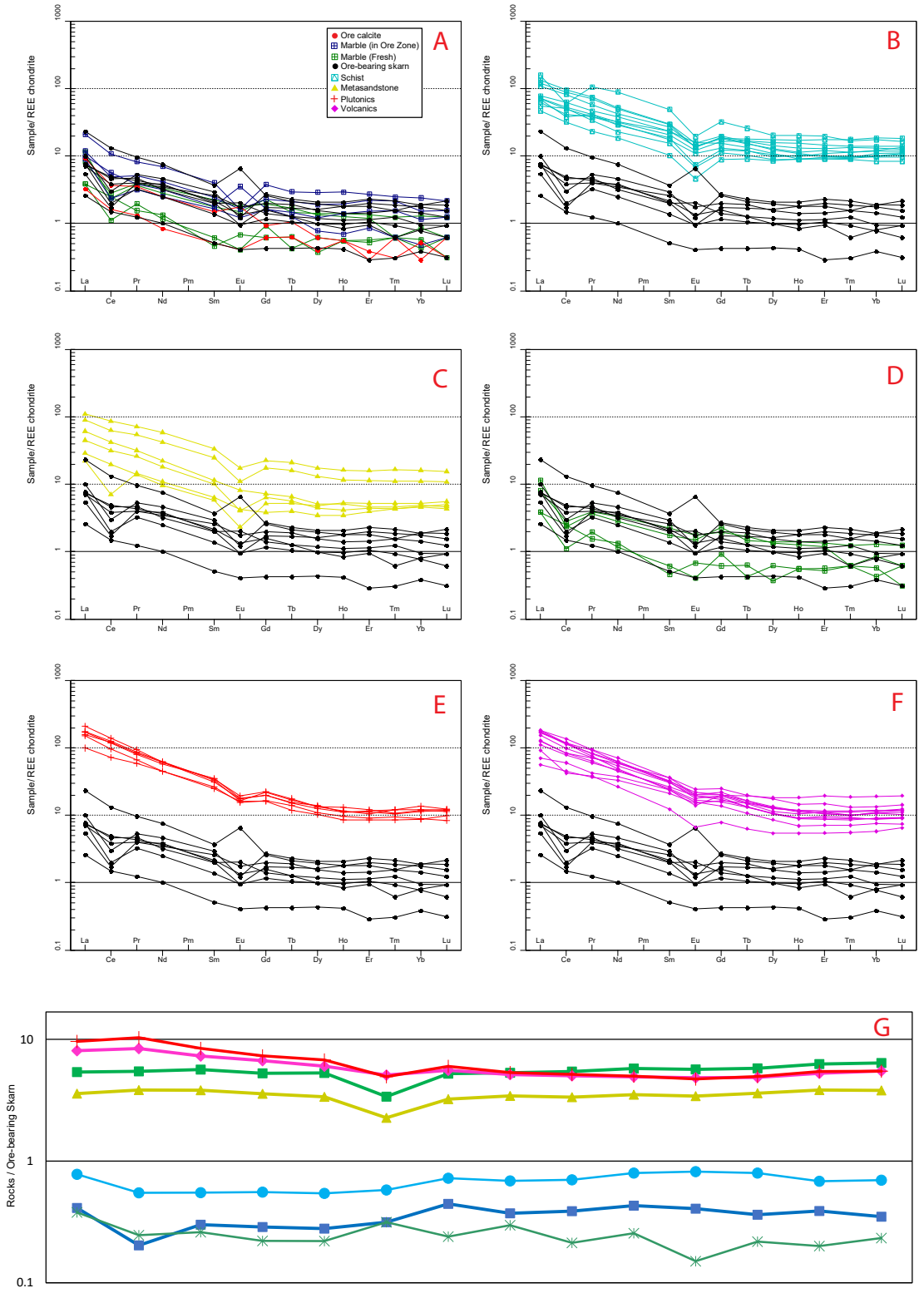


Figure 7. REE spider diagrams of the wall rocks and ore-bearing skarns. Chondrite normalized values were taken from Boynton (1984), a. ore-bearing skarn and all carbonate occurrences, b. ore-bearing skarn and schist, c. ore-bearing skarn and metasandstone, d. ore-bearing skarn and marble, e. ore-bearing skarn and plutonics, f. ore-bearing skarn and volcanics, g. average ore-bearing skarn-normalized average values of all wall rocks and carbonate occurrences.

are slightly higher in ore zone marble. When the ΣREE values of these carbonaceous occurrences are compared to those of the ore-bearing skarn samples (3.34–27.20 ppm, avg: 11.30 ppm, SD: 7.00, n:8), the ΣREE values of the ore-bearing skarn samples are similar to the ore zone marble and are also higher than the fresh marble and ore calcite. Chondrite-normalized (Boynton, 1984) REE plots of all carbonaceous occurrences (Figure 7a) show enrichments in LREE and a decrease towards middle rare earth elements (MREE). These values also exhibit a flat trend between MREE and HREE (Figure 7a). All the carbonate samples show consistent trends with each other; however, the ore calcite samples show an irregular trend in LREE. The REE trends of ore-bearing skarns and carbonaceous occurrences are compatible with each other (Figure 7a). Most of the fresh marble, ore zone marble, ore calcite, and ore-bearing skarn samples show negative Eu and Ce anomalies. One of the ore-bearing skarn samples exhibits a very strong positive while the other one exhibits a very strong negative Eu anomaly, and similar strong positive and negative anomalies are also observed in one marble region in the ore zone sample. Although there are minor fluctuations in REE concentrations in all of the samples, there is not much REE gain/loss during mineralization (Figure 7a).

The chondrite-normalized (Boynton, 1984) REE patterns of metamorphic rocks exhibit a similar trend (Figures 7b–7d). When the REE values compare to each other, slightly higher enrichment in LREE relative to MREE and HREE, and a flat trend between MREE and HREE are typical for metamorphic rocks (Figures 7b–7d). However, the normalized values of metasandstone and schist are about ten times higher than those of the fresh marble. The metamorphic rocks show a slightly negative Eu anomaly (Figures 7b–7d). The REE patterns of the ore-bearing skarns are compatible with those of all metamorphic rocks and enriched at the same proportion with fresh marble. In addition, almost all fresh marble samples, one metasandstone sample (CC07_2_35), and one schist sample (CC07_2_17) show negative Ce anomalies.

The general trend in the chondrite-normalized REE diagram of plutonic rocks (Figure 7e) indicates the high crustal contribution. The negative Eu anomaly reflects the probable plagioclase fractionation. The chondrite-normalized REE values of volcanic rocks (Figure 7f), HREE (flat-trends) and LREE enrichments are ten times and a hundred times higher, respectively than the chondrite values. The general trend observed here is also compatible with the general trend of plutonic rocks (Figures 7e and 7f). The REE patterns of igneous rocks are also compatible with those of ore-bearing skarns. However, REE enrichments of igneous rocks are ten times higher than those of ore-bearing skarns.

The ore-bearing skarns-normalized wall rocks diagram (Figure 7g) indicates that the fresh marble, the ore zone marble, and the ore calcite contain less REEs than ore-bearing skarns and are higher than that in the schist, metasandstone, and igneous rocks. The reference values are calculated using the average values of ore-bearing skarns in this study.

5.4. Compositional variation of skarn-related plutonic rocks

The geochemical features and compositional variation of subalkaline plutonic rocks in the Biga Peninsula indicate that these plutons evolved from the Eocene to the Oligo-Miocene (Delaloye and Bingöl, 2000; Altınkaynak and Dilek, 2006). The melt source(s), cooling histories, and tectono-magmatic evolutions of these plutons have been analyzed in detail (e.g., Altunkaynak and Dilek, 2006; Altunkaynak et al., 2012; Black et al., 2013; Aysal, 2015; Aydın et al., 2019). Therefore, the skarn formation potential of the plutons associated with Pb-Zn mineralizations are examined in this chapter.

The skarn-related plutons of the Biga Peninsula (this study; Genç and Altunkaynak, 2007; Akıska, 2010; Black, 2012; Aysal, 2015; Altunkaynak et al., 2012; Aydın et al., 2019) and the average values of worldwide skarn-related plutons from Meinert (1995) were evaluated in Figure 8. Almost all samples in the MgO-SiO_2 diagram (Figure 8a) were plotted near the Fe, Au, and Cu skarn plutons. The plutons in the K_2O-SiO_2 diagram (Figure 8b) were clustered around the field of Cu skarn plutons. The distribution of samples in the total alkali-SiO_2 (TAS) diagram (Figure 8c) and AFM diagram (Figure 8d) are similar to the distribution in Figures 8a and 8b. These samples are scattered around the Cu-Pb-Zn skarn plutons in the Al-saturation diagram (Figure 8e).

In the Sc-Rb binary diagram (Figure 8f), the Biga plutons were seen around the Cu, Au, and Pb-Zn skarn plutons. In the Ni-V diagram, the Biga plutons show a distribution far from the average values of the worldwide skarn-forming plutons (Meinert, 1995). However, they show partial closeness to Pb-Zn, Cu, and Au skarns (Figure 8g). The Biga plutons are generally clustered between Au and Cu and around the Pb-Zn skarn plutons in the Zr-Rb/Sr diagram (Figure 8h).

Based on the tectonic discrimination diagram, the Biga plutons are placed around the Cu- and Pb-Zn skarn plutons and fall into the post-COLG area (Figure 8i). These samples are also close to the average values of Au and Fe skarn plutons.

6. Sulfur isotopes

The frequency histogram and change intervals of the delta 34 sulfur isotope compositions obtained in this study and compiled from the literature (Örgün et al., 2005; Bozkaya,

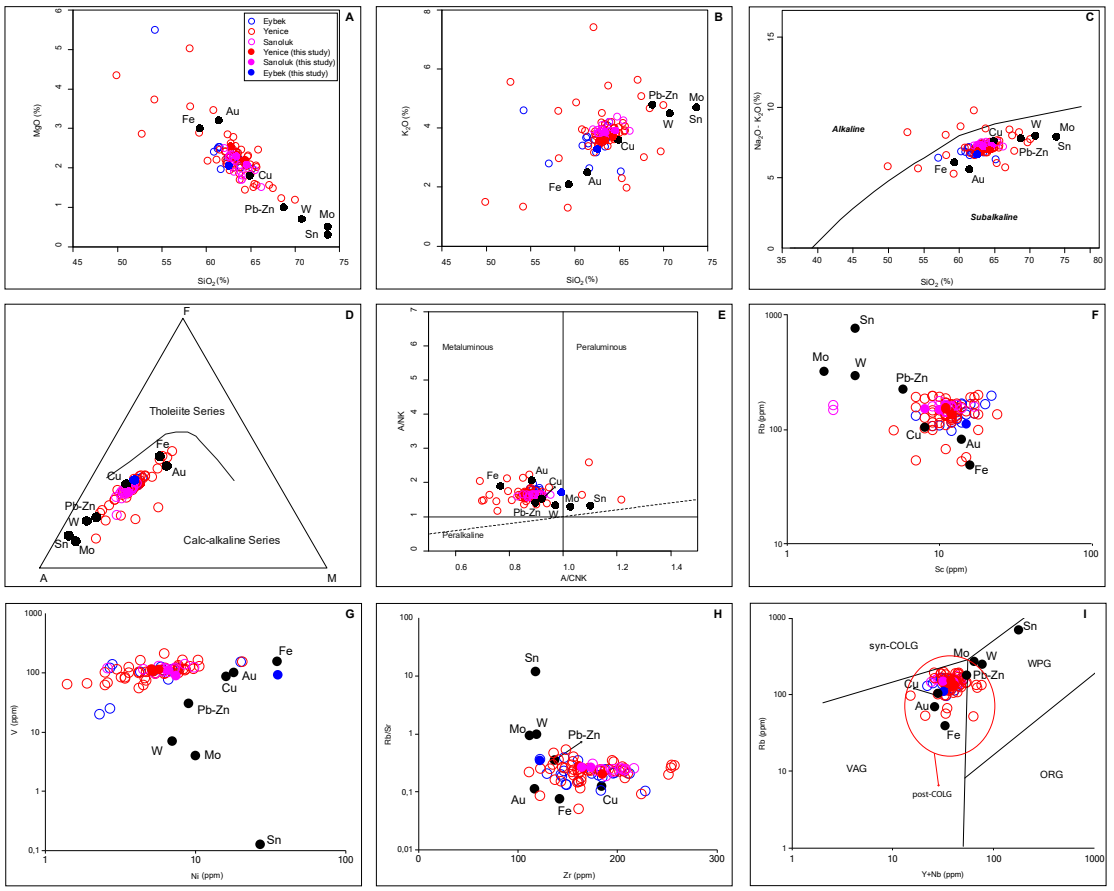


Figure 8. Representation of the average values of the skarn-forming plutons worldwide (Meinert, 1995) and the plutons in the Biga Peninsula. Major oxide Harker diagrams (a. SiO_2 vs. MgO, b. SiO_2 vs. K_2O), c. TAS diagram (Irvine and Baragar, 1971), e. Al-saturation diagram (Shand, 1943), trace element Harker diagrams (f. Sc vs. Rb, g. Ni vs. V, h: Zr vs. Rb/Sr), i. tectonic discrimination diagram (Pearce et al., 1984, Pearce, 1996). (*Abbreviations: ORG: ocean ridge granites, post-COLG: postcollisional granites, syn-COLG: syn-collisional granites, VAG: volcanic arc granites, WPG: within-plate granites.*) (*The pluton data taken from the literature belong to Akıska, 2010; Altunkaynak et al., 2012; Black, 2012; Aysal, 2015; Aydın et al., 2019.*)

2011; Akıska et al., 2013; Çiçek et al., 2021) can be seen in Figure 9 and the $\delta^{34}S$ isotope values of all regions in Table 7.

The $\delta^{34}S$ isotope values of the sulfide minerals from the Handeresi Ore District range between –1.20 and +3.54‰ (avg. +0.6‰, SD: 1.20, n: 44). Those of the Sameteli Ore District have an average $\delta^{34}S$ value of –4.2‰ that range between –5.5 and –2.6‰ (SD: 0.81, n: 8). Samples from the Alandere mineralization have $\delta^{34}S$ values that range from –3.2 to +0.1‰ (avg. –2.0‰, SD: 1.10, n: 9). The Arapuçandere deposit has $\delta^{34}S$ values within the range of –5.94 to 0.6‰ (avg. –2.90‰, SD: 1.60, n: 46) whereas the Kurttaşı mineralizations has $\delta^{34}S$ values within the range of –2.4 to 5.2‰ (avg. 0.1‰, SD: 2.27, n: 8). The S isotope values of all deposits are typically close to the Canon Diablo Troilite reference material and fall in a narrow range. All samples, with the exception of the Sameteli Ore District, range between –2.90 and +0.6‰. The $\delta^{34}S$ values of the Sameteli Ore District (avg. –4.2‰) are slightly lower than that of the others.

7. Discussion

7.1. Skarn formation conditions of Biga plutons

All samples from the Biga plutons in the Sakarya fragment plotted around the Fe, Au, and Cu skarn plutons on the MgO-SiO_2 and K_2O-SiO_2 diagrams (Figures 8a and 8b). However, major oxide Harker diagrams may not provide exact evidence for genesis, igneous processes, and mineralization (Meinert, 1995). To better understand the magmatic variations, these three components have to be understood; i) the main element compositions of rock-

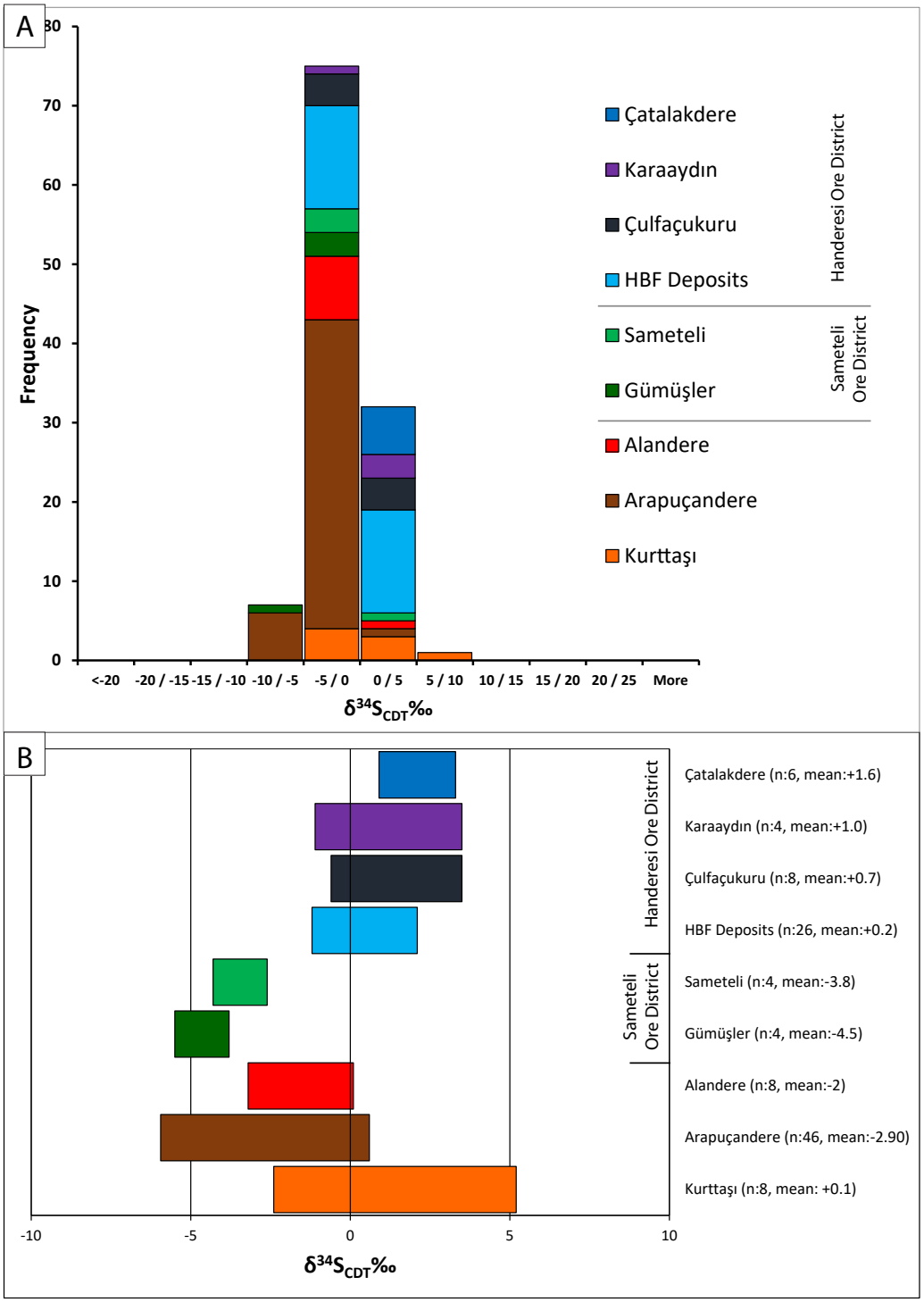


Figure 9. a. Frequency histogram, and b. the composite data of $\delta^{34}S$ values for sulfides.

forming minerals (e.g., Ebby, 1992); ii) rare mineral phases and the elements in accessory minerals (e.g., Piccoli and Candela, 1994), and iii) element substitutions in the main mineral phases (e.g., Arth, 1976). In addition, the trace elements used in igneous petrogenesis and their ratios are fundamental for understanding the basic principles (Pearce et al., 1984; Lightfoot et al., 1993; Meinert, 1995). As reported by Meinert (1995), skarn-related plutons

Table 7. $\delta^{34}S_{VCDT}$ isotope values of sulfide minerals and H_2S_{aq} in equilibrium with the sulfide minerals in Pb-Zn deposits of Biga Peninsula (n.i.e.: not in equilibrium).

			$\delta^{34}S$ (per mil)				$\delta^{34}S$-H_2S (per mil)[a]						
Sample#	**Area**	**Ore District**	**Galena**	**Sphalerite**	**Pyrite**	**Chalcopyrite**	**Galena**	**Sphalerite**	**Pyrite**	**Chalcopyrite**	Δ_{Sp-Gn}	**T (°C)[b]**	
CAT13-01	Çatalakdere	Handeresi Ore District	1.0	3.3	-	-	2.9	3.0	-	-	2.3	290.22	This study
CAT13-02	Çatalakdere		0.9	1.3	0.9	2.2	-	-	-	-	-	n.i.e.	
CC13-01	Çulfaçukuru		-	1.5	1.9		-	-	-	-	-	-	
CC13-02	Çulfaçukuru		−0.3	−0.4	0.3	−0.4	-	-	-	-	-	n.i.e.	
CC13-03	Çulfaçukuru		−0.6	-	3.5	-	-	-	-	-	-	-	
DD13-01	Karaaydın		-	0.8	3.5	-	-	-	-	-	-	-	
DD13-02B	Karaaydın		−1.1	0.6	-	-	0.3	0.4	-	-	1.7	388.66	
KD13-03	Kurttaşı		−2.4	0.6	0.0	−0.7	0.2	0.2	−1.6	−0.5	3.0	222.40	
KD13-04	Kurttaşı		−1.5	0.0	−0.3		−0.2	−0.2	−1.1		1.5	430.26	
KD13-05	Kurttaşı		-	-	-	5.2	-	-	-	-	-	-	
SAM13-01	Sameteli	Sameteli Ore District	−4.2	-	-		-	-	-	-	-	-	
SAM13-03	Sameteli		−4.3	-	-	−2.6	-	-	-	-	-	-	
SAM13-05	Sameteli		−4.3	-	-		-	-	-	-	-	-	
GUM13-02	Gümüşler		−5.5	−4.5	−4.1	−3.8	-	-	-	-	-	n.i.e.	
AD13-03	Alandere		−3.2		-	-	-	-	-	-	-	-	
AD13-04	Alandere		−2.8	−3.1	-	-	-	-	-	-	-	n.i.e.	
AD13-05	Alandere		−2.0	−2.7	−0.9	-	-	-	-	-	-	n.i.e.	
ÇK-2	Alandere		-	-	-	0.1	-	-	-	-	-	-	Çiçek et al. (2021)
ÇK-4	Alandere		−1.8	−1.7	-	-	-	-	-	-	-	n.i.e.	
ARP-3	Arapuçandere			0.6	-	-	-	-	-	-	-	-	
160-V4-9	Arapuçandere		−3.0	−0.8	-	−0.6	−1.0	−1.0	-	−0.5	2.2	295.90	
308-V4-1	Arapuçandere		−4.0	−1.8	-	−0.7	−2.1	−2.1	-	−0.6	2.2	297.80	
160-V5-3	Arapuçandere		−2.6	−0.3	-	−0.7	−0.6	−0.6	-	−0.5	2.3	292.30	
308-V5-3	Arapuçandere		−1.2	−1.2	-	−0.9	-	-	-	-	-	n.i.e.	

Table 7. (Continued)

			$\delta^{34}S$ (per mil)				$\delta^{34}S$-H_2S (per mil)[a]						
Sample#	**Area**	**Ore District**	**Galena**	**Sphalerite**	**Pyrite**	**Chalcopyrite**	**Galena**	**Sphalerite**	**Pyrite**	**Chalcopyrite**	Δ_{Sp-Gn}	**T (°C)[b]**	
1	Arapuçandere		–4.3	-	-	-	-	-	-	-	-	-	Orgün et al. (2005)
2	Arapuçandere		–3.6	-	-	-	-	-	-	-	-	-	
3	Arapuçandere		–4.2	-	-	-	-	-	-	-	-	-	
4	Arapuçandere		–3	-	-	-	-	-	-	-	-	-	
5	Arapuçandere		–5.2	-	-	-	-	-	-	-	-	-	
6	Arapuçandere		–5.1	-	-	-	-	-	-	-	-	-	
7	Arapuçandere		–3.8	-	-	-	-	-	-	-	-	-	
8	Arapuçandere		–2.4	-	-	-	-	-	-	-	-	-	
9	Arapuçandere		-	-	–1.9	-	-	-	-	-	-	-	
10	Arapuçandere		-	-	–2.2	-	-	-	-	-	-	-	
11	Arapuçandere		-	-	–2.5	-	-	-	-	-	-	-	
12	Arapuçandere		-	-	–3.4	-	-	-	-	-	-	-	
13	Arapuçandere		-	-	–1.2	-	-	-	-	-	-	-	

[a]: Calculated from the equations of Ohmoto and Rye (1979).

[b]: Calculated from sphalerite-galena pairs based on the equation of Ohmoto and Rye (1979) except Bağırkaçdere samples. Bağırkaçdere values are the homogenization temperatures of the sphalerite minerals (Akıska and Demirela, 2014).

Table 7. (Continued)

			$\delta^{34}S$ (per mil)				$\delta^{34}S$-H_2S (per mil)						
Sample#	**Area**	**Ore District**	**Galena**	**Sphalerite**	**Pyrite**	**Chalcopyrite**	**Galena**	**Sphalerite**	**Pyrite**	**Chalcopyrite**	Δ_{Sp-Gn}	**T (°C)**	
AUD-2	Arapuçandere		–4.18	–5.17	-	-	-	-	-	-	-	n.i.e.	Bozkaya (2001)
AUD-3	Arapuçandere		–4.22	–4.43	-	-	-	-	-	-	-	n.i.e.	
AUD-10	Arapuçandere		–3.73	–5.52	-	-	-	-	-	-	-	n.i.e.	
AUD-12	Arapuçandere		–3.37	-	-	–3.45	-	-	-	-	-	-	
AUD-23	Arapuçandere		–3.45	-	-	–2.44	-	-	-	-	-	-	
AUD-24	Arapuçandere		–5.94	-	-	–0.86	-	-	-	-	-	-	
AUD-25	Arapuçandere		–2.59	-	-	-	-	-	-	-	-	-	
AUD-26	Arapuçandere		–3.7	–1.74	-	-	–2.0	–2.0			2.0	337.14	
AUD-33	Arapuçandere		–5.26	-	-	-	-	-	-	-	-	-	
AUD-35	Arapuçandere		–4.6	-	-	–3.48	-	-	-	-	-	-	
AUD-36	Arapuçandere		–3.42	-	-	-	-	-	-	-	-	-	
AUD-40	Arapuçandere		–1.91	-	-	-	-	-	-	-	-	-	
HDHD1	Handeresi	Handeresi Ore District		-	-	0.2	-	-	-	-	-	-	Akıska et al. (2013)
HDK(p)	Handeresi		1.5	-	-	1.5	-	-	-	-	-	-	
HDK90	Handeresi		1	2.1	-	-	-	-	-	-	-	n.i.e.	
HDYU91	Handeresi		–1.2	0.4	-	-	0.2	0.2	-	-	1.6	402.31	
HDYU95	Handeresi		–0.8	-	-	-	-	-	-	-	-	-	
AB69	Bağırkaçdere		1.2	-	-	-	-	-	-	-	-	-	
BAG07_2	Bağırkaçdere		–0.7	-	-	-	-	-	-	-	-	-	
BG64	Bağırkaçdere		0.1	-	-	-	2.0	-	-	-	-	305.00	
BG66	Bağırkaçdere		–0.1	-	-	-	1.7	-	-	-	-	315.00	
BG68	Bağırkaçdere		–0.2	-	-	-	1.8	-	-	-	-	289.00	
BG70	Bağırkaçdere		1	-	-	-	3.1	-	-	-	-	272.00	
BG71	Bağırkaçdere		0.8	-	-	-	2.5	-	-	-	-	338.00	
BG72	Bağırkaçdere		–0.4	-	-	0.6	1.5	-	-	0.8	-	300.00	
FD07_1	Fırıncıkdere		–1.1	-	-	-	-	-	-	-	-	-	
FD07_2	Fırıncıkdere		–0.1	1.7	-	–0.6	1.5	1.5	-	–0.5	1.8	363.68	
FD07_3	Fırıncıkdere		–0.4	-	-	-	-	-	-	-	-	-	
FD11	Fırıncıkdere			–0.7	-	–0.4	-	-	-	-	-	-	
FD6	Fırıncıkdere		–0.1	0.8	-	-	-	-	-	-	-	n.i.e.	

are typically subalkaline in character based on the major element compositions (Figure 8c). Skarn-related plutons plot between the metaluminous-peraluminous areas and almost none are classified as peralkaline on the Al-saturation diagram (Meinert, 1984, 1995) (Figure 8e). When evaluated in terms of their geochemical characteristics and formation environments the plutons related to the Biga skarn deposits exhibit similar characteristics with the skarn-forming plutons (Black et al., 2013; Aysal, 2015; Aydın et al., 2019; Özdamar et al., 2021).

During the crystallization-differentiation, the Rb concentration should increase, and the Sc concentration should decrease as pyroxenes form relatively early and K-feldspar and muscovite form relatively late during the crystallization of granitic melts (Meinert, 1992, 1995) (Figure 8f). Sc, V, and Ni concentrations have the highest values in calcic-Fe skarn plutons, and these values gradually decrease towards Au, Cu, Zn, and W skarn plutons in worldwide skarns (Meinert, 1995) (Figures 8f and 8g). The Ni values of the Biga plutons (except Eybek pluton) have low values because of the mobility of nickel in superficial conditions (Figure 8g). The high Ni value of the Eybek pluton is due to the wall rocks that the pluton intruded into, rather than being a pluton associated with Fe skarn. Akıska (2010) noted the ophiolitic and ultramafic units that are seen in drill cores but not seen as outcrops in Handeresi area. Violarite, millerite, linneite, and chromite were detected in one of the samples that was collected in the ore adit in the Handeresi area (Akıska, 2010). It is likely that the Eybek pluton interacted with these units during its intrusion and assimilated some parts of them, causing the Ni value to increase. The relative effect of the differentiation may test on the Rb/Sr (highly sensitive to differentiation) vs. Zr diagram (Figure 8h). While the average Zr values of different skarn plutons worldwide do not differ significantly, the Rb/Sr values of these plutons related to W, Mo, and especially Sn skarns vary considerably (Meinert, 1995). The Biga plutons in this diagram have similar crystallization and differentiation features as those in the Rb-Sc diagram (Figure 8f).

Another use of trace element data is tectonic environment discrimination diagrams associated with distinct magma types (e.g., Pearce et al., 1984). The two most commonly used diagrams are Rb vs. (Y+Nb) and Nb vs. Y. The majority of plutons associated with skarns are formed in post-COLG, volcanic arcs and intracontinental areas. Fe, Au, and Cu skarns are typically associated with plutons in the post-COLG region, while Zn, Sn, W, and Mo skarns are associated with plutons in the intracontinental areas (Meinert, 1992). No plutons associated with skarn deposits fall within the area of ORG and syn-COLG (Figure 8i). The tectonic environment characteristics of the Biga plutons (Altunkaynak et al., 2012; Black et al., 2013; Aysal, 2015; Aydın et al., 2019) also support these inferences. According to these authors, Cenozoic magmatism in the Biga Peninsula occurred postdate the closure of the Neotethyan Ocean. When evaluated in terms of skarn-forming Biga plutons, all plutons were clustered close to each other in the post-COLG area (Figure 8i).

It is understood that the samples taken from the plutons associated with the mineralizations of the Biga Peninsula may represent the plutons that can create the Pb-Zn, Cu, Fe, and Au skarn in Figure 8. Although Pb-Zn mineralizations were considered in this study, there are also Cu, Fe, and Au skarn type mineralizations associated with the same plutons in the Biga Peninsula (e.g., Soğucak Fe-Cu skarn mineralization—Yenice pluton (Aysal et al., 2006; Çiçek et al., 2021); Evciler Au-Cu skarn mineralization—Evciler pluton (Öztürk and Helvacı, 2008)). Another significant finding is that the Biga plutons generally do not have the chemical composition to form Sn, W, and Mo skarns. Indeed, no Sn, W, and Mo skarn occurrences have been detected in the Biga Peninsula.

7.2. Element behaviors and effects on mineralization

Considering the geochemical characteristics of the igneous rocks, the increase and decrease in Sr values can be explained by possible weathering effects (Middelburg et al. 1988). Especially, the intensive arenization in granodiorite and intense argillization in volcanic rocks are the most important evidence of these weathering effects.

The high values of mineralization-related elements (e.g., Pb, Zn, Cu, Cd, Ag) in metasandstones indicate that these elements may be initially rich in the protolith of these rocks. The high values of As and Sb also support this view. Previous studies have argued that there may be some contributions from the wall rocks in the Biga mineralizations (e.g., Bozkaya and Gökçe, 2009; Akıska et al., 2013). For this reason, metasandstone may also be one of the wall rocks that provide the ore elements to the mineralization. Nb is related to the alkali metals (Na and K) and most Na and rich minerals other than plagioclase have high Y for their Ca contents (Lambert and Holland, 1974). The high values of the Nb can be explained by the fact that feldspar is the main rock-forming mineral, while the low values of the Y element may be due to the scarcity of phyllosilicate minerals in these rocks. The chemical differentiation on reference rock-normalized metasandstones is sourced from the different chemical characterization of the different sandstone types such as arkose, greywacke, and lithic sandstone. Reference rock values in the literature (e.g., Turekian and Wedepohl, 1961) are typically given as sandstones, but their types are not distinguished.

Fresh marbles have completely $CaCO_3$ content. Si, Fe, Mn, and Mg values are higher in marble and much higher in ore calcite than the fresh marble. It is expected that Si

and Fe will increase in the ore zone. However, two points stand out here. The first is the increase in the Mn value. The high manganese contents in the distal Pb-Zn skarn zone were reported by many researchers (e.g., Meinert, 1987; Yun and Einaudi, 1982; Meinert, 1992). On the other hand, Mn-oxide and Mn-hydroxide minerals such as pyrolusite, psilomelane, and manganite which are present especially in the Çulfa Çukuru deposit can also explain the high manganese content. The second is the inverse correlation between Mg and Mn. This behavior is explained by the opposite behaviors of these elements (Nakano, 1991; Nakano et al., 1994). This inverse correlation is typical for the skarn deposits. Especially in distal Pb-Zn skarn deposits, high Mn in the environment and accordingly low Mg are also typically observed especially in pyroxene (Nakano, 1991; Nakano et al., 1994). This inverse correlation is seen in two ore calcite samples in this study. Both in this study and previous studies on the Biga Pb-Zn deposits, it has been observed that the diopside mineral is rare, whereas Mn-hedenbergite and johannsenite minerals are abundant (Akıska et al., 2013, Demirela et al., 2014, Akıska, 2020).

Clustering methods are methods that make use of distance matrix or similarity matrix to create homogeneous and heterogeneous groupings between units or variables (Sharma, 1996). Hierarchical cluster analysis (or hierarchical clustering) is a general approach to cluster analysis where the object is to group together objects or records that are "closer" to each other. The result is graphically represented as a dendrogram. HCA is also used in ore deposits studies to understand whether elements move together and to group them. In this study, chemical analysis of ore-bearing skarn samples was performed to HCA analysis (Figure 10). Three different groups were detected in an HCA analysis of ore samples (80.22% of the total variation on the dataset is explained by three factors with principal component analysis). These groups were interpreted as the element group getting enriched in the environment during the alteration, the element group removed from the environment, and the element group forming the ore. The fact that the group formed by Ba and Sr was formed as a different group and the other findings above suggest that Ba, along with Sr, also removed from the environment (Figure 10). Sb, Rb, Zr, Ag, Y, Mo, Hg, and Nb were added to the environment by acting together. Cu, Au, As, Cd, and related Pb and Zn were also added during the mineralization stage. Cu, Pb, Zn, and As showing a positive anomaly and Sr showing a negative anomaly in ore-bearing schist sample suggests that the amount of Sr decreased during alteration and mineralization. The result of HCA is also consistent with the ore-bearing schist sample.

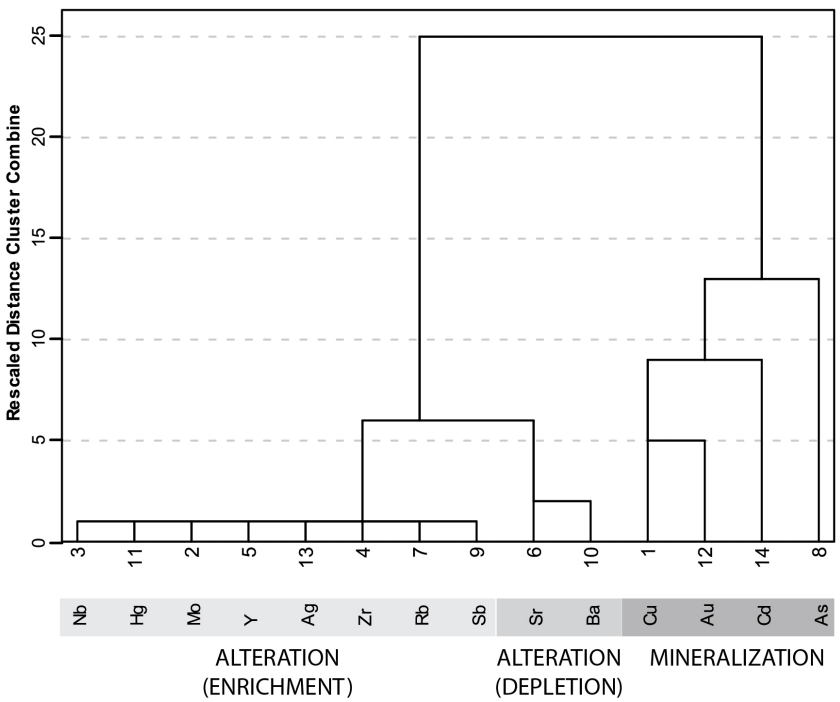


Figure 10. Hierarchical cluster analysis diagram showing element association during alteration/mineralization.

7.3. REE source(s) of ore and host rocks

Carbonate-bearing and other metamorphic units generally have negative Eu and Ce (mostly) anomalies even if they show small differences (Figures 7a–7d). Whitney and Olmsted (1998) found that negative Eu anomalies were inherited from protoliths, which may also be the case for this study. Since there is no obvious Eu anomaly in the plutonic rocks which are thought to be the main source of the ore fluid. The presence of negative Ce anomaly in both carbonate-bearing and other metamorphic units in the Sakarya fragment of the Biga Peninsula and the fact that the Ce content did not show a significant change in the skarn mineralization may reflect that the ancient seawater in which schist, marble, and metasandstone protoliths precipitated was remarkably poor in Ce (Kato, 1999). The REE chemistry of Ca-bearing minerals (e.g., calcite, fluorite) provides important information on metal sources, temperature conditions, fluid migration, water-rock interaction, and the chemical composition of the fluids (Bau et al., 2003; Schwinn and Markl, 2005; Castorina et al., 2008; Sánchez et al., 2010). Because Ca^{2+} in Ca-bearing minerals can easily be replaced by REE, REEs are easily enriched in Ca-bearing minerals (e.g., He et al., 2021). Y/Ho ratios of marble in ore zone and calcite in Biga Pb-Zn mineralizations vary in a narrow range between 34 and 55 (Table 5), indicating a hydrothermal origin (approximately 20–11; Bau and Dulski, 1995). However, Y/Ho ratios of fresh marble have similar values (40–55), which indicates that there is no significant loss/gain during mineralization.

The REE values of ore-bearing skarn are less than those of igneous rocks (Figures 7e and 7f). Akıska et al. (2013), Demirela et al. (2014), and Akıska (2020) indicated that meteoric water adds into the ore-bearing fluids while Pb-Zn skarn formations occur. The relative depletions in the REE values of ore-bearing skarn may be due to the addition of meteoric water. Likewise, it has been noted that meteoric water contributed to the mineralization fluids in the vein-type Pb-Zn deposits of the Biga Peninsula (Örgün et al., 2005, Bozkaya et al., 2008; Bozkaya and Gökçe, 2009; Bozkaya and Banks, 2015; Çiçek and Oyman, 2016).

Kato (1999) compared the REE values of skarn to wall rocks and normalized all wall rocks associated with the mineralization with skarn samples. The results obtained indicate that the normalized values of the wall rock (igneous rock) and marble were plotted around 1. According to Kato (1999), these two rocks were related to the skarn, and it has been hypothesized that there was not much REE loss/gain in the skarnization phase. The REE ratios of the wall rocks (except fresh marble) in the Biga Peninsula do not entirely reflect the REE ratios of the ore-bearing skarn samples (Figure 7). This finding can be interpreted as the mineralization lacking one single origin. Akıska et al. (2013), Akıska and Demirela (2014), and Akıska (2020) in their studies concerning the Pb-Zn occurrences in the Biga Peninsula noted that the ore samples were not only of magmatic origin but also contributed by the host rocks. In addition, Akıska and Demirela (2014) found based on the fluid inclusion characteristics that the mineralization is not only of magmatic origin but also meteoric water contribution. The authors also emphasized some carbon contribution from the reactive carbonates to the ore calcite.

Ore-bearing skarn samples have similar REE abundances and trends with fresh marble, whereas other metamorphic and igneous rocks have higher ΣREE values (Figures 7a–7f) (Table 5). Since igneous rocks are rich in aluminum, they have high REE concentrations (Kato, 1999), and thus, these high REE-bearing rocks are particularly insensitive to hydrothermal fluids with very low REE concentrations (Kato, 1993). The absence of significant changes in the REE indices during mineralization indicates that the ore-forming hydrothermal fluids have very low REE concentrations when compared to igneous rocks (Kato, 1993; Kato, 1999). In the Biga samples, the REE concentrations of carbonate-bearing rocks are ten times lower than the aluminum-bearing rocks (igneous rocks in this study). Marble is thought to be far more sensitive to fluids with low REE concentrations, and this provides valuable information on the REE values of hydrothermal fluids than high aluminum content rocks (Kato, 1999). Due to the low REE content of carbonate rocks, the water-rock interaction cannot significantly change the REE concentration in the hydrothermal fluid under conditions of low water/rock ratios (Haas et al., 1995). In the Biga samples, the REE patterns of ore-bearing skarn samples are similar to those of carbonate units (Figures 7a–7f). The decrease in ∑REE during the formation of skarn minerals from marble indicates that REE concentrations in the original hydrothermal fluids were low enough to weaken the REEs derived from marble or to mask the REE concentrations of marble. The similarity of the REE indices of ore calcite to marble also indicates that a significant amount of REEs in calcite is derived from marbles. This result is consistent with the C-O isotope values of Akıska and Demirela (2014).

The rock/ore-bearing (Figure 7g) skarn diagram indicates that some, if not significant, REE loss occurred in the carbonate-bearing rocks during mineralization. However, the REE ratios of ore calcite samples and fresh marble are similar to each other, indicating that this gain in the ore-bearing skarn zone is not reflected in ore calcites. All samples show a nearly flat profile, and the profile of ore zone marble is closer to ore-bearing skarns.

In skarn deposits, the $(Pr/Yb)_{cn}$, Ce/Ce*, and Eu/Eu* values increase as the ∑REE values increase, reflecting the REE characteristics of magmatic origin fluids (Kato, 1999; Zamanian and Radmard, 2016). In contrast, the REE

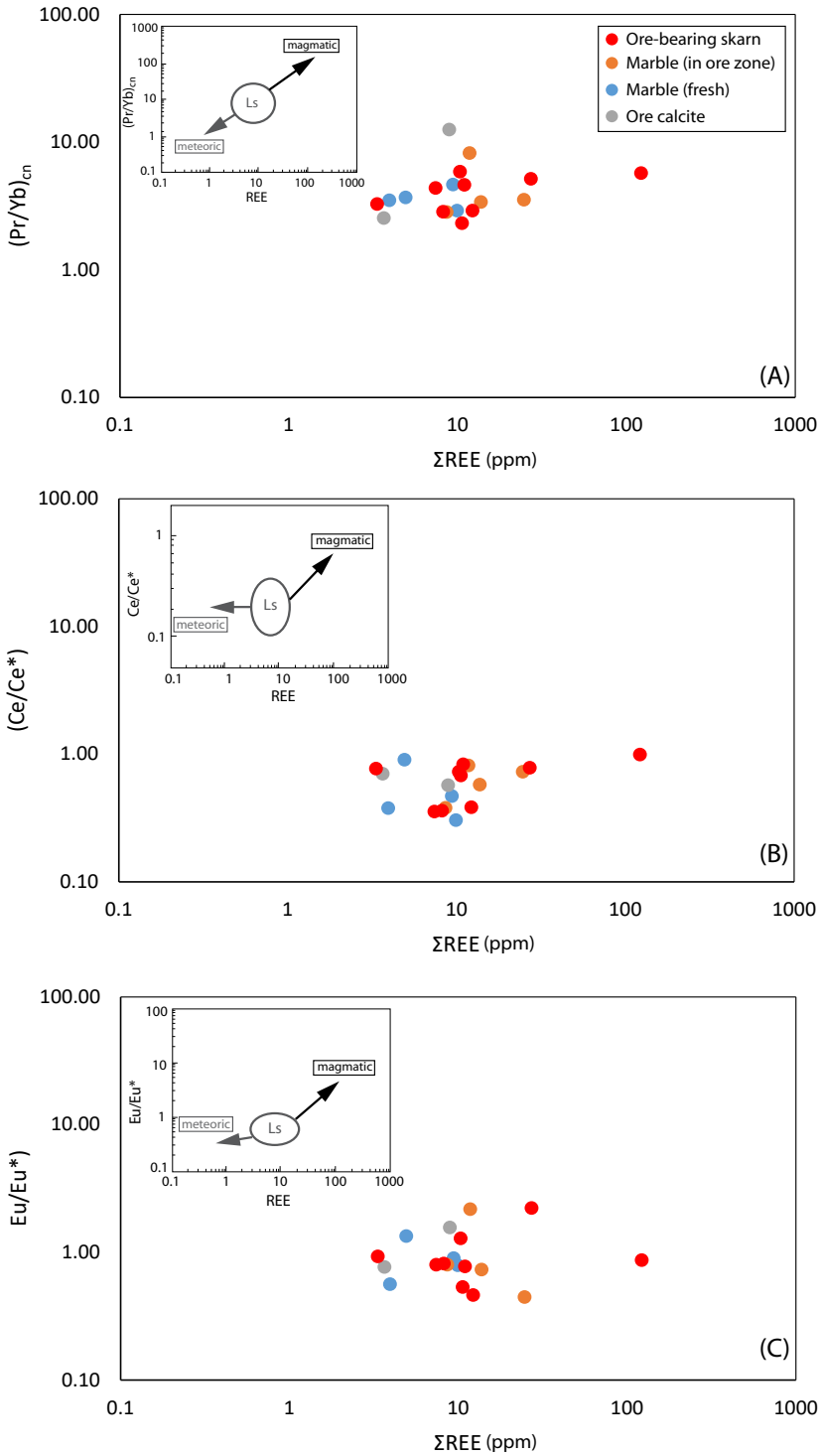


Figure 11. Binary diagrams (Kato, 1999) show changes of REE indices of carbonate-bearing samples in this study due to reaction with hydrothermal fluids of magmatic or meteoric origins.

concentrations of meteoric water are significantly lower. For this reason, although the $(Pr/Yb)_{cn}$ ratios decrease as the ∑REE values decrease in the deposits formed by meteoric water, there is no significant change in Ce/Ce* and Eu/Eu* values (Kato, 1999). As can be seen in Figures 11a–11c, meteoric water contributed to the fluids forming the mineralization in the Biga-Sakarya fragment Pb-Zn deposits. This result, as stated previously, is in agreement with the results obtained by previous isotope, mineral chemistry, and fluid inclusion studies (e.g., Bozkaya et al., 2008; Akıska et al., 2013; Bozkaya and Banks, 2015; Akıska, 2020).

7.4. Evolution of the ore-forming system

Sphalerite chemistry is important for recording the temperature and fS_2 evolution of the ore-forming system (Frenzel et al., 2022 and references therein). Using equilibrium temperature (Akıska and Demirela, 2014) and mol% FeS–mol% ZnS values in sphalerite (Akıska, 2020), the samples were interpreted on the fS_2-T diagram for the paths of the ore-forming fluids (Figure 12a). The fS_2 values were calculated based on the equation of Frenzel et al. (2022). The sphalerite samples lie within the field of intermediate-sulfidation (IS) epithermal systems in the diagram (Figure 12a). The Arapuçandere epithermal deposit, which is a well-studied deposit in the region, is defined as of intermediate-sulfidation epithermal type (Çiçek et al., 2021). Similarly, the Handeresi Ore District and Kurttaşı base metal mineralizations are formed under intermediate-sulfidation conditions. In addition, the evolutionary trend of the sphalerite samples began from the "gas-buffer" within the porphyry-Cu deposits field and followed the "rock buffer" of Einaudi et al. (2003) (Figure 12a). This trend indicates that the ore-forming fluids cooled in equilibrium with the wall rocks, such as metamorphic and igneous rocks. This also implies that, in addition to mixing with meteoric and/or sea waters, the observed changes in ore-forming conditions are the main driving force (Einaudi et al., 2003; Voudouris et al., 2008).

However, the ratio (the SO_2/H_2S gas ratio) may increase on phase separation due to the loss of H_2S and H_2 to the vapor or due to sulfide deposition, or may decrease as a result of chemical exchange with wall rocks containing ferrous iron or carbonaceous matter (Ohmoto and Rye, 1979). Considering the absence of sulfate minerals in the study areas and the ore-bearing components carried by H_2S-rich fluids precipitated in a reducing environment (Akıska, 2020), the fact that the volatiles took carbonaceous material from the host rocks (Akıska and Demirela, 2014) also played an important role in the decrease in the SO_2/H_2S rate.

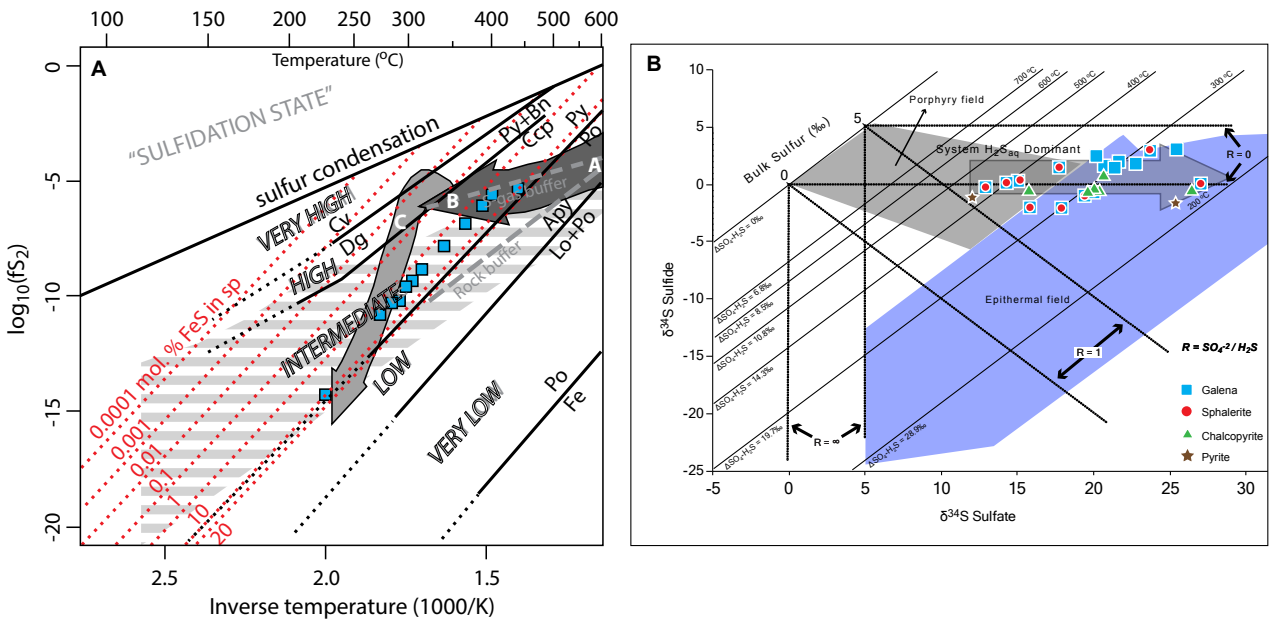


Figure 12. a. Log fS_2 – 1000 / T (°K) diagram defining the relative sulfidation state of hydrothermal fluids (Einaudi et al., 2003). The Main Line (horizontal thick grey lines) ore-forming environment from Barton (1970), and the evolutionary path of fluids in porphyry copper and porphyry-related vein deposits ("Lazy-L" shaped). Mol %Fe in sphalerite lines were given from Frenzel et al. (2022). Sulfidation reactions from Barton and Skinner (1979), b. δsulfate-δsulfide diagram of the Biga Pb-Zn mineralizations. S isotopic data of porphyry and transition/intermediate sulfidation epithermal deposits (pH = 4-5) from the model of equilibrium fractionation of sulfur isotopes between sulfide and sulfate in ore-bearing fluids (Hutchinson et al., 2020). *Abbreviations: apy = arsenopyrite; bn = bornite; ccp = chalcopyrite; cv = covellite; dg = digenite; fe = iron; lo = loellingite; po = pyrrhotite; py = pyrite.*

7.5. Isotope equilibrium and geothermometry

A sulfur isotopic fractionation process may be triggered by either kinetic or chemical processes. The process of fractionation between compounds containing sulfur will follow the chemical composition and temperature of the fluid source (Ohmoto and Rye, 1979; O'Neil, 1986; Seal, 2006). The mineral grains that were analyzed (galena and sphalerite) were selected from the adjacent mineral grains. These mineral pairs were precipitated simultaneously. For this reason, the analyzed galena-sphalerite pairs can be considered as coexisting minerals. The details of the ore microscopy studies of galena-sphalerite pairs were performed by Örgün et al. (2005), Akıska (2010), Bozkaya (2011), Akıska et al. (2013), Akıska (2020). The $\delta^{34}S$ isotope values of the sulfides in this study decrease in the order pyrite, chalcopyrite, sphalerite, and galena even if their values are close to one another ($\delta^{34}S_{pyrite\text{-}avg.}$: –0.5‰, SD: 2.35, $\delta^{34}S_{chalcopyrite\text{-}avg.}$: –0.6‰, SD: 2.09, $\delta^{34}S_{sphalerite\text{-}avg.}$: –0.8‰, SD: 2.33,$\delta^{34}S_{galena\text{-}avg.}$: –2.2‰, SD: 2.04). It is difficult to say with the data whether isotopic equilibrium has been obtained or not; however, there are several studies on sphalerite fluid inclusions in the literature. The homogenization temperature of the sphalerite was measured as 228–272 °C for the Handeresi Ore District (Akıska and Demirela, 2014) and 229–384 °C (Örgün et al., 2005; Bozkaya et al., 2008) for the Arapuçandere mineralization. The 9 mineral pairs obtained from the sphalerite-galena geothermometry show an equilibrium temperature range of 222.40–402.31 °C, which is consistent with the fluid inclusion homogenization temperatures.

The $\delta^{34}S_{sulfide}$-$\delta34S_{sulfate}$ diagram (Fifarek and Rye, 2005; Rye, 2005; Seal, 2006; Marini et al., 2011) can be used to predict the redox states, $\delta^{34}S_{\Sigma S}$ composition, and SO_4^{2-}/H_2S ratios of ore-bearing fluids (Rye, 1993, 2005; Bethke et al., 2005; Hutchinson et al., 2020). Although no sulfate minerals were observed in the study areas, this diagram can also be constructed with the aid of equilibrium temperature data calculated with the $\delta^{34}S$ isotope compositions and the data obtained from the fluid inclusion homogenization temperatures (Li et al., 2016; Çiçek et al., 2021). The H_2S_{aq} values in equilibrium with sulfides were calculated by using S isotope geothermometry (Table 7) obtained from the galena-sphalerite pairs and $\delta^{34}S$ values of other sulfide minerals (pyrite and chalcopyrite) formed at the equilibrium temperature (equations of Ohmoto and Rye, 1979). In addition, the fluid inclusion homogenization temperature values of sphalerites in the Bağırkaçdere mineralization (Akıska and Demirela, 2014) were also used.

The $\delta^{34}S$ values of H_2S_{aq}, which is in equilibrium with the sulfide minerals in the study areas, ranged from –2.1 to 3.1‰ (Table 7). Although epithermal Pb-Zn and distal skarn Pb-Zn mineralizations are observed in the study areas, it has been stated in previous studies (Akıska, 2010; Akıska et al., 2013; Akıska and Demirela, 2014; Akıska, 2020; Çiçek et al., 2021) that the formation conditions, time, and ore mineral characteristics of both types of deposits are similar, and the mineralization environments have the same physicochemical characteristics. The $\delta^{34}S$ isotope data of the sulfides in this study also support this observation. There was no significant difference in the $\delta^{34}S$ isotope and the H_2S_{aq} values according to the deposit types. The most significant difference between both types of deposits is the characteristics of the host rocks (Akıska et al., 2013; Akıska and Demirela, 2014; Akıska, 2020). In the study carried out on the Biga Pb-Zn distal skarns by Akıska (2020), it was stated that the mineralizations were formed under 10–12 MPa pressure. Based on the studies mentioned above and the data obtained in this study, the mineralizations took place on the thermodynamic model (Hutchinson et al., 2020) in accordance with the low sulfidation-transition/intermediate zones with near neutral pH model among the appropriate redox buffer zones (Figure 12b). A few samples belonging to the Handeresi Ore District are seen in the porphyry area and the other samples are aligned along the H_2S dominated reduced line (R = 0) (Figure 12b). This suggests that the fluids associated with the surrounding porphyry systems are likely to be H_2S-rich under relatively reducing conditions. These data are also compatible with the result of the EPMA study by Akıska (2020) which argues that mineralizations are formed in a reducing environment. According to these data, it is believed that the mineralizations in the Handeresi Ore District may be spatially associated with the Tepeoba Cu-Mo porphyry deposit and the Kurttaşı Pb-Zn mineralization with the Taztepe Cu-Mo porphyry mineralization.

7.6. Source of sulfur in the ores

The S isotope values of all the deposits are typically close to 0 and lie in a narrow range with the exception of the Sameteli Ore District. The $\delta^{34}S$ values of the Sameteli Ore District ($\delta^{34}S_{avg}$: –4.2‰) are slightly lower than the others. The Sameteli Ore District mineralizations were formed at the contact of the schist and the marbles and are both lithologically and structurally controlled. During the field studies, andesite, dacite, tuff and porphyric rocks were found to be exposed in areas close to mineralization. In these areas, the units have intense hydrothermal alteration. However, Yenigün (1980) stated that hydrothermal quartz lodes with a 5-m-thick comb-like texture were detected around the porphyric rocks, and the same textures were also observed in the ore-bearing lodes. It was argued by the author that the mineralization may originally be related to volcanics. The reason for the slightly low sulfur isotope values in the region may be the addition of bacterial sulfur to the magmatic sulfur in the mineralization or a mixture from a reservoir with depleted S isotope composition. However, in many studies with similar S isotope values, sulfur was originally determined as magmatic. While

Ohmoto and Rye (1979) stated in their study that values between –3 and +3‰ are of magmatic origin, it has been stated by Bowman (1998) that they generally take values between –5 and +5‰ in Zn skarn deposits. The Sameteli Ore District mineralizations along with the Alandere and the Handeresi Ore District mineralizations are similar to each other, both temporally and spatially (Akıska, 2010, Akıska et al., 2013, Akıska, 2020). For this reason, it is thought that sulfur in ore-forming fluids may also be of magmatic origin.

8. Conclusion

Based on the wall rock lithological features, structural elements of the mineralizations, isotope, mineral chemistry, and fluid inclusion studies of ore and alteration minerals, the Biga Sakarya fragment Pb-Zn deposits are classified as Pb-Zn skarns (dominantly distal type) and hydrothermal (intermediate sulfidation) Pb-Zn deposits. Schist, metasandstone, marble, volcanic rock, granitoid and ore-bearing alteration zones were outcropped in the study areas.

According to the results of the skarn potential of the Biga plutons diagrams, these plutons have chemical characteristics that can form Pb-Zn, Cu, Fe, and Au skarns. These results are approved by the presence of similar skarns and the absence of Sn, W, and Mo skarns in the Biga Peninsula.

Three different groups of elements were detected on the HCA results of ore-bearing samples: i) elements increasing in the environment (Sb, Rb, Zr, Ag, Y, Mo, Hg, and Nb), ii) elements away from the environment (Sr and Ba), and elements forming the mineralization during alteration (Cu, Au, As, and Cd).

The geochemical characteristics of the carbonate-bearing samples indicate the increase of the Si, Fe, Mn, and Mg values from fresh marble to the ore calcite. The high quantities of Mn in distal Pb-Zn skarn deposits worldwide and the presence of manganese oxide minerals (e.g., pyrolusite, psilomelane) in the study area (e.g., Çulfa Çukuru area) can also account for the increase in Mn.

When the schist samples are compared to the ore-bearing schist sample, Cu, Pb, Zn, and As increase and Sr decreases in the ore-bearing schist sample. The scarcity of Sr is also compatible with the data obtained from the HCA. The fact that the elements associated with mineralization in the metasandstone are relatively high indicates that this rock group may also contribute to the mineralization.

It appears that carbonates in the Biga Pb-Zn deposits are of hydrothermal origin and the REE decrease in ore-bearing samples is sourced from the meteoric water in the ore-bearing fluids. The fact that the REE values of the wall rocks differ from the REE values in the ore-bearing skarn samples indicate that the fluids forming the mineralization are not of a single origin. There appeared no significant loss/gain in the REE content of carbonate rocks during the formation of ore-bearing skarn minerals. The REE indices of ore calcites are similar to marble, suggesting that a significant amount of REEs in calcite is derived from marble.

According to the REE characteristics of the wall rocks, the hydrothermal fluids responsible for the formation of the Biga Peninsula Pb-Zn deposits are characterized by very low REE concentrations, and as a result, the origin of these fluids is predominantly of meteoric origin. The data obtained from the $(Pr/Yb)_{cn}$, Ce/Ce*, and Eu/Eu* diagrams also confirms this result. In addition, based on the similarities of the general REE trends and abundances of ore-bearing skarn samples with those of different rock groups along with igneous rocks, it was concluded that there may be contributions from host rocks during mineralization.

According to the $\delta^{34}S$ values, the mineralizations in the study areas occurred under intermediate sulfidation conditions, in a reducing environment with H_2S-dominant fluids with a pH value of about 4–5. The source of the sulfur forming the sulfide mineralizations in the region is magmatic.

Acknowledgments

The authors would like to thank Halim Mutlu and İ. Sönmez Sayılı for providing constructive and positive contributions that improved the manuscript. We thank Orhan Tatar (Editor-in-chief), associate editor, and anonymous reviewers for their helpful comments. This study was supported by Scientific Research Office of Ankara University (BAPRO) under grant number 13B4343009.

References

Akıska S (2010). Cu-Pb-Zn occurrences of the Yenice (Çanakkale) Area. Ph.D. Thesis, Ankara University pp. 234 Ankara (in Turkish with English abstract, unpublished).

Akıska S, Demirela G (2014). Origin of the Fluids in the Handeresi, Bağırkaçdere, and Fırıncıkdere (Kalkım, Yenice-ÇANAKKALE) Pb-Zn±Cu Distal Skarn Deposits. Yerbilimleri 35 (3): 199-218 (in Turkish with English abstract). https://doi.org/10.17824/huyuamd.90366

Akıska S, Sayılı İS, Demirela G (2013). Geology, mineralogy and the Pb, S isotope study of the Kalkım Pb-Zn±Cu deposits, Biga Peninsula, NW Turkey. Journal of Geosciences 58 (4): 379-396. http://doi.org/10.3190/jgeosci.154

Akıska S (2020). Crystallization conditions and compositional variations of silicate and sulfide minerals in the Pb-Zn skarn deposits, Biga Peninsula, NW Turkey. Ore Geology Reviews 118: 103322. https://doi.org/10.1016/j.oregeorev.2020.103322

Aldanmaz E, Koprubasi N, Gurer ÖF, Kaymakci N, Gourgaud A (2006). Geochemical constraints on the Cenozoic, OIB-type alkaline volcanic rocks of NW Turkey: implications for mantle sources and melting processes. Lithos 86: 50-76. https://doi.org/10.1016/j.lithos.2005.04.003

Aldanmaz E, Pearce J, Thirlwall MF, Mitchell J (2000). Petrogenetic evolution of late Cenozoic, post-collision volcanism in western Anatolia, Turkey. Journal of Volcanology and Geothermal Research 102 (1-2): 67-95. https://doi.org/10.1016/S0377-0273(00)00182-7

Altunkaynak Ş (2007). Collision-driven slab breakoff magmatism in Northwestern Anatolia, Turkey. Journal of Geology 115: 63-82. https://doi.org/10.1086/509268

Altunkaynak Ş, Dilek Y (2006). Timing and nature of postcollisional volcanism in western Anatolia and geodynamic implications. In: Dilek, Y., Pavlides, S. (Eds.), Post collisional tectonics and magmatism in theMediterranean region and Asia: Geological Society of America Special Paper 409: 321-351. https://doi.org/10.1130/2006.2409(17)

Altunkaynak Ş, Genç ŞC (2008). Petrogenesis and time-progressive evolution of the Cenozoic continental volcanism in the Biga Peninsula, NW Anatolia (Turkey). Lithos 102: 316-340. https://doi.org/10.1016/j.lithos.2007.06.003

Altunkaynak Ş, Sunal G, Aldanmaz E, Genç CŞ, Dilek Y et al (2012). Eocene Granitic Magmatism in NW Anatolia (Turkey) revisited: New implications from comparative zircon SHRIMP U-Pb and 40Ar-39Ar geochronology and isotope geochemistry on magma genesis and emplacement. Lithos 155: 289-309. https://doi.org/10.1016/j.lithos.2012.09.008

Anıl M (1984). Genesis of the Pb-Zn-Cu mineralizations and relations with Tertiary volcanism in Yenice area (Arapuçandere-Kurttaşı, Sofular and Kalkım-Handeresi). Jeoloji Mühendisliği Dergisi 8 (2): 19-30 (in Turkish with English abstract).

Arth JG (1976). Behavior of trace-elements during magmatic processes - a summary of theoretical models and their applications. Journal of Research of the U.S. Geological Survey 4 (1): 41-47.

Aydın Ü, Şen P, Özmen Ö, Şen E (2019). Petrological and geochemical features of Biga Peninsula granitoids, NW Anatolia, Turkey. Bulletin of the Mineral Research and Exploration 160: 81-115. https://doi.org/10.19111/bulletinofmre.466522

Aygül M, Topuz G, Okay AI, Satır M, Meyer HP (2012). The Kemer Metamorphic Complex (NW Turkey), a subducted continental margin of the Sakarya zone. Turkish Journal of Earth Sciences 21: 19-35. https://doi.org/10.3906/yer-1006-14

Aysal N (2015). Mineral chemistry, crystallization conditions and geodynamic implications of the Oligo-Miocene granitoids in the Biga Peninsula, Northwest Turkey. Journal of Asian Earth Sciences 105: 68-84. https://doi.org/10.1016/j.jseaes.2015.03.026

Aysal N, Öngen S, Hanilçi N (2006). Petrography of the contact zone rocks and features of the skarn formation of Karadoru granitoid pluton, Yenice-Çanakkale. İstanbul Üniversitesi Mühendislik Fakültesi Yerbilimleri Dergisi 19 (2): 183-194 (in Turkish with English abstract).

Aysal N, Öngen AS, Şahin SY, Kasapçı C, Hanilçi N et al (2021). Peritectic assemblage entrainment and mafic-felsic magma interaction in the Late Oligocene-Early Miocene Karadağ Pluton in the Biga Peninsula, northwest Turkey: petrogenesis and geodynamic implications. Turkish Journal of Earth Sciences 30(2): 279-312. https://doi.org/10.3906/yer-2005-6

Barton PB Jr, (1970). Sulfide petrology: Mineralogical Society of America, Special Paper No. 3, p. 187-198.

Barton PB Jr, Skinner BJ (1979). Sulfide mineral stabilities, in Barnes, H. L., ed., Geochemistry of hydrothermal ore deposits, Second Edition: New York, Holt, John Wiley & Sons, p. 278-403.

Bau M, Romer RL, Lüders V, Dulski P (2003). Tracing element sources of hydrothermal mineral deposits: REE and Y distribution and Sr-Nd-Pb isotopes in fluorite from MVT deposits in the Pennine Orefield England. Mineralium Deposita 38: 992-1008. https://doi.org/10.1007/s00126-003-0376-x

Bau M, Dulski P (1995). Comparative study of yttrium and rare-earth element behavior in fluorine-rich hydrothermal fluids. Contributions to Mineralogy and Petrology 119: 213-223. https://doi.org/10.1007/BF00307282

Beccaletto L, Jenny C (2004). Geology and correlation of the Ezine Zone: a Rhodope fragment in NW Turkey? Turkish Journal of Earth Sciences 13: 145-176.

Beccaletto L, Bartolini AC, Martini R, Hochuli PA, Kozur H (2005). Biostratigraphic data from the Cetmi Melange, northwest Turkey: paleogeographic and tectonic implications. Palaeogeography, Palaeoclimatology, Palaeoecology 221: 215-244. https://doi.org/10.1016/j.palaeo.2005.02.011

Beccaletto L, Bonev N, Bosch D, Bruguier O (2007). Record of a Palaeogene syn-collisional extension in the north Aegean Sea: evidence from the Kemer micaschists (NW Turkey). Geological Magazine 144: 393-400. https://doi.org/10.1017/S001675680700310X

Bethke PM, Rye RO, Stoffregen RE, Vikre PG (2005). Evolution of the magmatic-hydrothermal acid-sulfate system at Summitville, Colorado: Integration of geological, stable-isotope, and fluid-inclusion evidence. Chemical Geology 215: 281-315. https://doi.org/10.1016/j.chemgeo.2004.06.041

Black KN, Catlos EJ, Oyman T, Demirbilek M (2013). Timing Aegean extension: evidence from in situ U-Pb geochronology and cathodoluminescence imaging of granitoids from NW Turkey. Lithos 180-181: 92-108. https://doi.org/10.1016/j.lithos.2013.09.001

Boynton WV (1984). Cosmochemistry of the rare earth elements: meteorite studies. In: Rare Earth Element Geochemistry, P. Henderson (ed.). Elsevier, 63-114, Amsterdam.

Bozkaya G (2011). Sulphur- and lead-isotope geochemistry of the Arapuçandere lead-zinc- copper deposit, Biga Peninsula, Northwest Turkey. International Geology Review 53 (1): 116-129. https://doi.org/10.1080/00206810902945090

Bozkaya G, Banks AD (2015). Physico-chemical controls on ore deposition in the Arapucandere Pb-Zn-Cu-precious metal deposit, Biga Peninsula. NW Turkey. Ore Geology Reviews 66: 65-81. https://doi.org/10.1016/j.oregeorev.2014.10.014

Bozkaya G, Gökçe A (2009). Lead and sulfur isotope studies of the Koru (Çanakkale, Turkey) lead-zinc deposits. Turkish Journal of Earth Sciences 18: 127-137.

Bozkaya G, Gökçe A, Grassineau NV (2008). Fluid Inclusion and Stable Isotope Characteristics of the Arapuçandere Pb-Zn-Cu Deposits, Northwest Turkey. International Geology Review 50 (9): 848-862. https://doi.org/10.2747/0020-6814.50.9.848

Castorina F, Masi U, Padalino G, Palomba M (2008). Trace-element and Sr-Nd isotopic evidence for the origin of the Sardinian fluorite mineralization (Italy). Applied Geochemistry 23: 2906-2921. https://doi.org/10.1016/j.apgeochem.2008.04.005

Cavazza W, Okay AI, Zattin M (2009). Rapid early-middle Miocene exhumation of the Kazdağ Massif (western Anatolia). International Journal of Earth Sciences 98: 1935-1947. https://doi.org/10.1007/s00531-008-0353-9

Çağatay A (1980). Geology and mineralogy of western Anatolian lead-zinc deposits and some comments about their genesis. Türkiye Jeoloji Kurumu Bülteni 23 (2): 119-132 (in Turkish with English abstract).

Çiçek M, Oyman T, Palmer MR (2021). Variation of Cu, Fe, S and Pb isotopes in sulfides from hydrothermal mineralization from the Yenice region in Çanakkale, Biga Peninsula, NW Turkey. Ore Geology Reviews 136: 104255. https://doi.org/10.1016/j.oregeorev.2021.104255

Çiçek M, Oyman T (2016). Origin and evolution of hydrothermal fluids in epithermal Pb-Zn-Cu ± Au ± Ag deposits at Koru and Tesbihdere mining districts, Çanakkale, Biga Peninsula. NW Turkey. Ore Geology Reviews 78: 176-195. https://doi.org/10.1016/j.oregeorev.2016.03.020

Delaloye M, Bingöl E (2000). Granitoids from western and northwestern Anatolia: geochemistry and modeling of geodynamic evolution. International Geology Review 42 (3): 241-268. https://doi.org/10.1080/00206810009465081

Demirela G (2011). Geology and genesis of the Çataltepe (Lapseki/Çanakkale) Pb- Zn±Cu±Ag Deposit. PhD Thesis, Ankara University 220 pp. Ankara (in Turkish with English abstract, unpublished).

Demirela G, Akıska S, Sayılı İS, Kuşcu İ (2014). Geology and the alteration features of the Çataltepe (Lapseki-Çanakkale) Pb-Zn±Cu±Ag deposit. Yerbilimleri 35 (2): 109-136 (in Turkish with English abstract).

Demirela G, Akıska S (2022). Evaluation of Pb isotope systematics and metal sources of the Biga Pb-Zn Province (NW Turkey) and comparison with the Pb isotope systematics of the Rhodope Massif. Journal of African Earth Sciences 187: 104445. https://doi.org/10.1016/j.jafrearsci.2021.104445

Dilek Y, Altunkaynak Ş, Öner Z (2009). Syn-extensional granitoids in the Menderes core complex, and the late Cenozoic extensional tectonics of the Aegean province. Journal of Geological Society London, Special Publications 321: 197-223. https://doi.org/10.1144/SP321.1

Dönmez M, Akçay AE, Genç ŞC, Acar Ş (2005). Middle-Late Eocene volcanism and marine ignimbrites in Biga Peninsula (NW Anatolia-Turkey). Bulletin of the Mineral Research and Exploration 131: 49-61 (in Turkish with English abstract).

Dönmez M, Akçay AE, Duru M, Ilgar A, Pehlivan Ş (2008). Geological map of the Çanakkale-H17 Quadrangle. MTA Publications no. 101, Ankara.

Duru M, Pehlivan Ş, Şentürk Y, Yavaş F, Kar H (2004). New results on the lithostratigraphy of the Kazdağ Massif in Northwest Turkey. Turkish Journal of Earth Sciences 13: 177-186.

Duru M, Pehlivan Ş, Okay Aİ, Şentürk Y, Kar H (2012) Pre-Tertiary geology of Biga Peninsula. MTA Special Report Series No. 28, Ankara, pp. 7–74 (in Turkish).

Einaudi MT, Hedenquist JW, Inan EE (2003). Sulfidation state of fluids in active and extinct hydrothermal systems: transition from porphyry to epithermal environments. In: Simmons SF, Graham I (eds) Volcanic, geothermal, and ore-forming fluids: rulers and witnesses of processes within the Earth, SEG Special Publication, vol. 10, Society of Economic Geologists, Littleton, Co., pp. 285-313. https://doi.org/10.5382/SP.10.15

Erkül F (2010). Tectonic significance of synextensional ductile shear zones within the Early Miocene Alaçamdağ granites, northwestern Turkey. Geological Magazine 147 (4): 611-637. https://doi.org/10.1017/S0016756809990719

Fifarek RH, Rye RO (2005). Stable-isotope geochemistry of the Pierina high-sulfidation Au-Ag deposit, Peru: Influence of hydrodynamics on SO_4^{2-}-H_2S sulfur isotopic exchange in magmatic-steam and steam-heated environments. Chemical Geology 215: 253-279. https://doi.org/10.1016/j.chemgeo.2004.06.040

Frenzel M, Voudouris P, Cook NJ, Ciobanu CL, Gilbert S et al. (2022). Evolution of a hydrothermal ore-forming system recorded by sulfide mineral chemistry: a case study from the Plaka Pb-Zn-Ag Deposit, Lavrion, Greece. Mineralium Deposita 57: 417-438. https://doi.org/10.1007/s00126-021-01067-y

Genç ŞC, Yılmaz Y (1997). An example of post-collisional magmatism in Northwestern Anatolia: the Kızderbent volcanics (Armutlu peninsula, Turkey). Turkish Journal of Earth Sciences 6: 33-42.

Güleç N (1991). Crust-mantle interaction in western Turkey: implications from Sr and Nd isotope geochemistry of Tertiary and Quaternary volcanics. Geological Magazine 128 (5): 417-435. https://doi.org/10.1017/S0016756800018604

Haas JR, Shock EL, Sassani DC (1995). Rare earth elements in hydrothermal systems: Estimates of standard partial molal thermodynamic properties of aqueous complexes of the rare earth elements at high temperatures and pressures. Geochimica et Cosmochimica Acta 59 (21): 4329-4350. https://doi.org/10.1016/0016-7037(95)00314-P

Harris NBW, Kelley S, Okay Aİ (1994). Post-collisional magmatism and tectonics in northwest Anatolia. Contributions to Mineralogy and Petrology 117: 241-252. https://doi.org/10.1007/BF00310866

He Z, Li Z, Li B, Chen J, Xiang Z et al (2021). Ore genesis of the Yadu carbonate-hosted Pb-Zn deposit in Southwest China: Evidence from rare earth elements and C, O, S, Pb, and Zn isotopes. Ore Geology Reviews 131: 104039. https://doi.org/10.1016/j.oregeorev.2021.104039

Herron MM (1988). Geochemical classification of terrigenous sands and shales from core or log data. Journal of Sedimentary Research 58 (5): 820-829. https://doi.org/10.1306/212F8E77-2B24-11D7-8648000102C1865D

Huston DL (1999). Stable isotopes and their significance for understanding the genesis of volcanic-hosted massive sulfide deposits: A review. Reviews in Economic Geology 10: 151-180. https://doi.org/10.5382/Rev.08.07

Hutchinson W, Finch AA, Boyce AJ (2020). The sulfur isotope evolution of magmatic-hydrothermal fluids: insights into ore-forming processes. Geochimica et Cosmochimica Acta 288: 176-198. https://doi.org/10.1016/j.gca.2020.07.042

Karacık Z, Yılmaz Y, Pearce JA, Ece OI (2008). Petrochemistry of the south Marmara granitoids, northwest Anatolia. Turkey. International Journal of Earth Sciences 97: 1181-1200. https://doi.org/10.1007/s00531-007-0222-y

Kato Y (1993). REE geochemistry of aluminous skarn in the representative Japanese skarn deposits. Resource Geology Special Issue 15: 393-400.

Kato Y (1999). Rare Earth Elements as an indicator to origins of skarn deposits: Examples of the Kamioka Zn-Pb and Yoshiwara-Sannotake Cu(–Fe) deposits in Japan. Resource Geology 49 (4): 183-198. https://doi.org/10.1111/j.1751-3928.1999.tb00045.x

Ketin İ (1966). Tectonic units of Anatolia (Asia Minor). Bulletin of the Mineral Research and Exploration 66: 23-34.

Köprübaşı N, Aldanmaz E (2004). Geochemical constraints on the petrogenesis of Cenozoic I-type granitoids in Northwest Anatolia, Turkey: evidence for magma generation by lithospheric delamination in a post-collisional setting. International Geology Review 46 (8): 705-729. https://doi.org/10.2747/0020-6814.46.8.705

Kuşcu İ, Tosdal RM, Gençalioğlu-Kuşcu G (2019). Episodic porphyry Cu (-Mo-Au) formation and associated magmatic evolution in Turkish Tethyan collage. Ore Geology Reviews 107: 119-154. https://doi.org/10.1016/j.oregeorev.2019.02.005

Lambert RSJ, Holland JG (1974). Yttrium geochemistry applied to petrogenesis utilizing calcium-yttrium relationships in minerals and rocks. Geochimica et Cosmochimica Acta 38 (9): 1393-1414. https://doi.org/10.1016/0016-7037(74)90095-7

Le Bas MJ, Le Maitre RW, Streckeisen A, Zanettin B (1986). A chemical classification of volcanic rocks based on the total alkali - silica diagram. Journal of Petrology 27 (3): 745-750. https://doi.org/10.1093/petrology/27.3.745

Li JX, Qin KZ, Li GM, Evans NJ, Zhao JX et al. (2016). The Nadun Cu-Au mineralization, central Tibet: root of a high sulfidation epithermal deposit. Ore Geology Reviews 78: 371-387. https://doi.org/10.1016/j.oregeorev.2016.04.019

Lightfoot PC, Hawkesworth CJ, Hergt J, Naldrett AJ, Gorbachev NS et al. (1993). Remobilisation of the continental lithosphere by a mantle plume; major-, trace-element, and Sr-, Nd-, and Pb isotope evidence from picritic and tholeiitic lavas of the Noril'sk District, Siberian Trap, Russia. Contributions to Mineralogy and Petrology 114: 171-188. https://doi.org/10.1007/BF00307754

Marini L, Moretti R, Accornero M (2011). Sulfur isotopes in magmatic-hydrothermal systems, melts, and magmas. Reviews in Mineralogy and Geochemistry 73 (1): 423-492. https://doi.org/10.2138/ rmg.2011.73.14

Meinert LD (1984). Mineralogy and petrology of iron skarns in western British Columbia, Canada. Economic Geology 79 (5): 869-882. https://doi.org/10.2113/gsecongeo.79.5.869

Meinert LD (1987). Skarn zonation and fluid evolution in the Groundhog mine, Central mining district, New Mexico. Economic Geology 82 (3): 523-545. https://doi.org/10.2113/gsecongeo.82.3.523

Meinert LD (1992). Skarns and skarn deposits. Geoscience Canada 19 (4): 145-162.

Meinert LD (1995). Compositional variation of igneous rocks associated with skarn deposits-chemical evidence for a genetic connection between petrogenesis and mineralization. Mineralogical Association of Canada. Short Course Series 23: 401-418.

Middelburg JJ, Van Der Weijden CH, Woittiez JRW (1988). Chemical processes affecting the mobility of major, minor and trace elements during weathering of granitic rocks. Chemical Geology 68: 253-273. https://doi.org/10.1016/0009-2541(88)90025-3

Middlemost EAK (1994). Naming materials in the magma/igneous rock system. Earth- Science Reviews 37: 215-224. https://doi.org/10.1016/0012-8252(94)90029-9

Nakano T (1991). An antipathetic relation between the hedenbergite and johannsenite components in skarn clinopyroxene from the Kagata tungsten deposit, Central Japan. The Canadian Mineralogist 29 (3): 427-434.

Nakano T, Yoshino T, Shimazaki H, Shimizu M (1994). Pyroxene composition as an indicator in the classification of skarn deposits. Economic Geology 89 (7): 1567-1580. https://doi.org/10.2113/gsecongeo.89.7.1567

O'Neil JR (1986). Theoretical and experimental aspects of isotopic fractionation. Stable Isotopes in High Temperature Geologic Process. In: Reviews in Mineralogy 16: 1-40. https://doi.org/10.1515/9781501508936-006

Ohmoto H, Rye RO (1979). Isotopes of sulfur and carbon. In: Barnes, HL (Ed.), Geochemistry of Hydrothermal Ore Deposits, second ed. Wiley, New York, pp. 509-567

Okay Aİ (1984). Distribution and characteristics of the north-west Turkish blueschists. Geological Society, London, Special Publications 17 (1), 455-466. https://doi.org/10.1144/GSL.SP.1984.017.01

Okay Aİ (1989). Tectonic units and sutures in the Pontides, northern Turkey. In: Tectonic evolution of the Tethyan region. Şengör A.M.C. (ed). NATO ASI Series (259), 109-116

Okay Aİ, Satır M (2000a). Coeval plutonism and metamorphism in a latest Oligocene metamorphic core complex in northwest Turkey. Geological Magazine 137 (5): 495-516. https://doi.org/10.1017/S0016756800004532

Okay Aİ, Satır M (2000b). Upper Cretaceous Eclogite-Facies Metamorphic Rocks from the Biga Peninsula, Northwest Turkey. Turkish Journal of Earth Sciences 9: 47-56.

Okay Aİ, Siyako M, Bürkan KA (1990). Geology and tectonic evolution of the Biga Peninsula. TPJD Bülteni 2 (1): 83-121 (in Turkish with English abstract).

Orhan A, Mutlu H (2017). Geochemical characteristics and Rare-earth element distributions of Kozbudaklar W-Skarn deposit (Bursa, Western Anatolia). Bulletin of the Mineral Research and Exploration 155: 115-130. https://doi.org/10.19111/bulletinofmre.305992

Örgün Y, Gültekin AH, Önal A (2005). Geology, mineralogy and fluid inclusion data from the Arapucan Pb-Zn-Cu-Ag deposit, Canakkale, Turkey. Journal of Asian Earth Sciences 25 (4): 629-642. https://doi.org/10.1016/j.jseaes.2004.06.006

Özdamar Ş, Roden MF, Zou H, Billor MZ, Hames W et al. (2021). Petrogenesis of oligocene plutonic rocks in western Anatolia (NW Turkey): Insights from mineral and rock chemistry, Sr-Nd isotopes, and U-Pb, Ar-Ar and (U-Th)/He geochronology. Geochemistry 81 (2): 125747. https://doi.org/10.1016/j.chemer.2021.125747

Öztürk YY, Helvacı C (2008). Skarn alteration and Au-Cu mineralization associated with Tertiary granitoids in Northwestern Turkey: Evidence from the Evciler Deposit, Kazdağ Massif, Turkey. Economic Geology 103 (8): 1665-1682. https://doi.org/10.2113/gsecongeo.103.8.1665

Pearce JA, Harris, NBW, Tindle AG (1984). Trace-element discrimination diagrams for the tectonic interpretation of granitic rocks. Journal of Petrology 25 (4): 956-983. https://doi.org/10.1093/petrology/25.4.956

Pearce JA (1996). Sources and Settings of Granitic Rocks. Episode 19 (4): 120-125. https://doi.org/10.18814/epiiugs/1996/v19i4/005.

Piccoli PM, Candela PA (1994). Titanite microchemistry and the interpretation of magmatic and hydrothermal processes in granitic systems. Abstracts with Programs – Geological Society of America 27 (7): 499.

Qicong L, Congqiang L (2003). Geochemical behaviors of REE and other trace elements during the formation of strata-bound skarns and related deposits: A case study of the Dongguashan Cu (Au) deposit, Anhui Province, China. Acta Geological Sinica – English Edition 77 (2): 246-257. https://doi.org/10.1111/j.1755-6724.2003.tb00568.x

Rye RO (1993). The evolution of magmatic fluids in the epithermal environment: the stable isotope perspective. Economic Geology 88 (3): 733-752. https://doi.org/10.2113/gsecongeo.88.3.733

Rye RO (2005). A review of the stable-isotope geochemistry of sulfate minerals in selected igneous environments and related hydrothermal systems. Chemical Geology 215: 5-36. https://doi.org/10.1016/j.chemgeo.2004.06.034

Rye RO, Ohmoto H (1974). Sulfur and Carbon Isotopes and ore genesis: A review. Economic Geology 69 (6): 826-842. https://doi.org/10.2113/gsecongeo.69.6.826

Sánchez V, Cardellach E, Corbella M, Vindel E, Martín-Crespo T et al. (2010). Variability in fluid sources in the fluorite deposits from Asturias (N Spain): further evidences from REE, radiogenic (Sr, Sm, Nd) and stable (S, C, O) isotope data. Ore Geology Reviews 37 (2): 87-100. https://doi.org/10.1016/j.oregeorev.2009.12.001

Schwinn G, Markl G (2005). REE systematics in hydrothermal fluorite. Chemical Geology 216: 225-248. https://doi.org/10.1016/j.chemgeo.2004.11.012

Seal RR II (2006). Sulfur isotope geochemistry of sulfide minerals. Reviews in Mineralogy and Geochemistry 61 (1): 633-677. https://doi.org/10.2138/rmg.2006.61.12

Seyitoğlu G, Scott B (1992). Late Cenozoic volcanic evolution of the northeastern Aegean region. Journal of Volcanology and Geothermal Research 54: 157-176. https://doi.org/10.1016/0377-0273(92)90121-S

Seyitoğlu G, Scott B (1996). The cause of N-S extensional tectonics in western Turkey: tectonic escape vs. backarc spreading vs. orogenic collapse. Journal of Geodynamics 22: 145-153. https://doi.org/10.1016/0264-3707(96)00004-X

Sharma S (1996) Applied multivariate techniques, John Wiley and Sons, Inc., New York, 512 pp.

Siyako M, Bürkan KA, Okay Aİ (1989). Tertiary geology and hydrocarbon potential of the Biga and Gelibolu peninsulas. TPJD Bülteni 1 (3): 183-200 (in Turkish with English abstract).

Şengör AMC, Yılmaz Y (1981). Tethyan evolution of Turkey: a plate tectonic approach. Tectonophysics 75: 181-241. https://doi.org/10.1016/0040-1951(81)90275-4

Şengün F, Çalık A (2007). Metamorphic Features and Correlation of the Çamlıca Metamorphics (Biga Peninsula, NW Turkey). Türkiye Jeoloji Bülteni 50: 1-16 (in Turkish with English abstract).

Şengün F, Yigitbaş E, Tunç İO (2011). Geology and tectonic emplacement of eclogite and blueschist, Biga Peninsula, Northwest Turkey. Turkish Journal of Earth Sciences 20: 273-285.

Tao R, Runsheng H, Yuzhao H (2012). REE Characteristic of Hydrothermal Calcite in Langdu Skarn Copper Deposit. Advanced Materials Research 524-527: 184-189.

Taylor HP Jr (1997). Oxygen and hydrogen isotope relationships in hydrothermal mineral deposits. In: Barnes HL (ed.) Geochemistry of Hydrothermal Ore Deposits, 3rd ed., pp. 229-302. New York, NY: Wiley.

Taylor Y, McLennan SM (1985). The Continental Crust: Its Composition and Evolution. Blackwell, Oxford, 312 pp.

Taylor SR (1969). Abundance of chemical elements in the continental crust: a new table. Geochimica et Cosmochimica Acta 28 (8): 1273-1285. https://doi.org/10.1016/0016-7037(64)90129-2

Tomascak PB (2004). Developments in the understanding and application of lithium isotopes in the earth and planetary sciences. Reviews in Mineralogy and Geochemistry 55(1): 153-195. https://doi.org/10.2138/gsrmg.55.1.153

Turekian KK, Wedepohl KH (1961). Distribution of the Elements in Some Major Units of the Earth's Crust. GSA Bulletin 72 (2): 175-192. https://doi.org/10.1130/0016-7606(1961)72[175:DOTEIS]2.0.CO;2

Voudouris P, Melfos V, Spry PG, Bonsall TA, Tarkian M et al. (2008). Mineralogical and fluid inclusion constraints on the evolution of the Plaka intrusion-related ore system, Lavrion, Greece. Mineralogy and Petrology 93: 79-110. https://doi.org/10.1007/s00710-007-0218-0

Wagner GA, Pernicka E, Seeliger TC, Öztunalı Ö, Baranyi I et al. (1985). Geologische untersuchungen zur fruhen metallurgie in NW-Anatolien. Bulletin of the Mineral Research and Exploration 100 (101): 45-81 (in German with English abstract).

Whitney PR, Olmsted JF (1998). Rare earth element metasomatism in hydrothermal systems: The Willsboro-Lewis wollastonite ores, New York, USA. Geochimica et Cosmochimica Acta 62 (17): 2965-2977. https://doi.org/10.1016/S0016-7037(98)00230-0

Yaltırak C, Okay Aİ (2004). Geology of the Paleotethys units at the northern part of Edremit Bay. İTÜ Dergisi 3 (1): 67-79 (in Turkish with English abstract).

Yılmaz Y (1989). An approach to the origin of young volcanic rocks of western Turkey. In: Sengör, A.M.C. (Ed.), Tectonic Evolution of the Tethyan Region: The Hague. Kluwer Academic, pp. 159-189.

Yılmaz Y (1990). Comparison of young volcanic associations of western and eastern Anatolia under compressional regime; a review. Journal of Volcanology and Geothermal Research 44: 69-87.

Yılmaz Y, Genç SC, Gürer OF, Bozcu M, Yılmaz K et al. (2000). When did the western Anatolian grabens begin to develop? In: Bozkurt, E., Winchester, J.A., Piper, J.A.D. (Eds.), Tectonics and Magmatism in Turkey and the Surrounding Area: Geol Soc London, Special Publication 173: 353-384. https://doi.org/10.1144/GSL.SP.2000.173.01.17

Yılmaz Y, Polat A (1998). Geology and evolution of the Thrace volcanism, Turkey. Acta Vulcanologica 10: 293-303.

Yiğit Ö (2012). A prospective sector in the Tethyan Metallogenic Belt: Geology and geochronology of mineral deposits in the Biga Peninsula. NW Turkey. Ore Geology Reviews 46: 118-148. https://doi.org/10.1016/j.oregeorev.2011.09.015

Yun S, Einaudi MT (1982). Zinc-lead skarns of the Yeonhwa Ulchin district, South Korea. Economic Geology 77 (4): 1013-1032. https://doi.org/10.2113/gsecongeo.77.4.1013

Zamanian H, Radmard K (2016). Geochemistry of rare earth elements in the Baba Ali magnetite skarn deposit, western Iran - a key to determine conditions of mineralization. Geologos 22 (1): 33-47. https://doi.org/10.1515/logos-2016-0003